Optimization of Part Consolidation for Minimum Production Costs and Time Using Additive Manufacturing

Zhenguo Nie[†], Sangjin Jung[†], Levent Burak Kara[†], Kate S. Whitefoot[*†‡]
[†]Mechanical Engineering, Carnegie Mellon University
[‡]Engineering and Public Policy, Carnegie Mellon University
Pittsburgh, PA, USA

ABSTRACT
This research presents a method of optimizing the consolidation of parts in an assembly using metal additive manufacturing (MAM). The method generates candidates for consolidation, filters them for feasibility and structural redundancy, finds the optimal build layout of the parts, and optimizes which parts to consolidate using a genetic algorithm. Results are presented for both minimal production time and minimal production costs, respectively. The production time and cost models consider each step of the manufacturing process, including MAM build, post-processing steps such as support-structure removal, and assembly. It accounts for costs affected by part consolidation, including machine costs, material, scrap, energy consumption, and labor requirements. We find that developing a closed-loop filter that excludes consolidation candidates that are structurally redundant with others dramatically reduces the number of candidates, thereby significantly reducing convergence time. Results show that, when increasing the number of parts that are consolidated, the production cost and time at first decrease due to reduced assembly steps, and then increase due to additional support structures needed to uphold the larger, consolidated parts. We present a rationale and evidence justifying that this is an important tradeoff of part consolidation that generalizes to many types of assemblies. Subsystems that are smaller, or can be oriented with very little support structures, or have low material costs or fast deposition rates can have an optimum at full consolidation; for other subsystems, the optimum is less than 100%. The presented method offers a promising pathway to minimize production time and cost by consolidating parts using MAM. In our test-bed results for an aircraft fairing produced with powder-bed electron-beam melting, the solution for minimizing production cost (time) is to consolidate 17 components into four (two) discrete parts, which leads to a 20% (25%) reduction in unit production cost (time).

Keywords: part consolidation, metal additive manufacturing, production cost and time, additive manufacturing optimization, design for additive manufacturing, closed-loop filter, genetic algorithm.

1. INTRODUCTION
Part consolidation is a design change in which multiple components that were formerly discrete and assembled together are fabricated as a single part. Through part consolidation, it is possible to reduce weight and size, minimize assembly operations, improve performance, and prolong service life [1]. Multiple demonstrations of part consolidation (referred to as consolidation hereafter) in industry have realized substantial reductions of production or lifecycle costs, weight reductions of up to 60%, and improved reliability [2].

Currently, it is difficult for researchers and manufacturers to identify promising opportunities to redesign products for consolidation using additive manufacturing (AM)[3]. Redesign for consolidation is done on an ad-hoc basis without systematically characterizing the effects of consolidating particular parts on assembly operations, production costs and time, or other manufacturer objectives. Complicating matters, determining which parts to consolidate is a combinatorial problem that explodes to large numbers of possible candidates even for assemblies with relatively few parts.

This research develops the first method that optimizes which parts to consolidate in an assembly using AM. Given a user-provided assembly design, the method seeks to minimize costs or time across the production process consisting of AM setup and build; finishing steps, including support structure removal; and assembly (if needed). Production costs are determined using a process-based cost model that considers equipment, material, and energy inputs; labor; and rejected parts. The method includes six stages to find the optimally consolidated design: generating candidates for consolidation using a connectivity matrix, filtering the candidates, optimizing the orientation and layout of parts during build, determining the AM build processing parameters, estimating the production costs and time for the design candidates, and finding the optimal design.

In the presented methodology, we develop a new filter that eliminates candidate designs for consolidation that are structurally redundant, meaning that for all practical considerations in manufacturing, they are identical to another candidate design. Specifically, if two candidate designs result in an identical set of parts that are each fabricated as monolithic structures whether or not one of the original

[*] Corresponding author: kwhitefoot@cmu.edu

interfaces in the part is consolidated, one of the candidate designs is removed from consideration.

The optimal design can be obtained for assemblies with a small number of parts by iterating over all candidates. For assemblies with many parts, we develop a genetic algorithm that encodes the part-interfaces that are consolidated in the candidate designs to find a solution with lower computational time.

We demonstrate the methodology on a test-bed assembly selected in collaboration with a company in the aircraft industry. The assembly is a titanium fairing that is produced by electron beam melting (EBM). Results indicate that using powder-bed fusion (PBF), the solution for minimizing production time is to consolidate 17 components into two parts, which leads to a 25% reduction in production time. The solution for minimizing production costs is to consolidate the components into four parts, leading to a 20% reduction in production costs.

These results illustrate an important tradeoff between the number of consolidated parts and the support structures that are needed during the build, which increase production costs and time. For many types of assemblies, it is easier to orient each individual component to reduce support structures than it is to orient consolidated parts because the parts are now larger and have more complex geometry. Consequently, as the number of consolidated parts increases, the total production cost (or time) at first decreases due to the elimination of assembly steps, and then increases due to increased cost (or time) associated with building and removing support structures. Because of these tradeoffs, it is not always optimal to consolidate the entire assembly even when it is feasible to do so.

We provide evidence justifying that this is an inherent tradeoff between consolidation and support structures that apply to many types of assemblies. If the geometry of the assembly is such that it can be oriented with minimal support structures when consolidated, the size of the assembly is relatively small, or the material cost is low (e.g., aluminum wire rather than titanium powder), the optimal number of consolidated parts can be 100%. In other cases, the optimal degree of consolidation is less than 100% even when full consolidation is feasible.

2. LITERATURE REVIEW

Benefits of consolidation. Consolidation can create several advantages in product performance and production, including simplified or eliminated assembly operations, reduced part weight and size, and improved structural performance. Existing literature has recognized the potential for consolidation to lead to significant cost savings from eliminating assembly operations and from the potential to optimize a product for the purpose in mind without compromising the design for assembly reasons [4]. Consolidation using AM has been demonstrated in multiple research case studies [2-3] and industries, including aerospace [5], automotive [6], and energy [7]. Yang et al. [2] studied the consolidation of a triple clamp, reducing part count from 19 to 7 with a weight reduction of 20% and demonstrated better performance. Schmelzle et al. [7] found that consolidation could reduce a hydraulic manifold's weight by 60% and height by 53% while improving performance and minimizing leak points. General Electric consolidated 230 parts in a compressor bladed disk of a turbine engine to one single part, leading to substantially lower lifecycle costs, 5-10% lower weight, and improved reliability and simplified maintenance [8]. Türk et al. [9] developed a new AM aircraft instrument panel that, compared to the previous design, reduced the number of parts by 50%, and total weight by 41%.

Constraints and tradeoffs with consolidation. Although consolidation has many benefits, it also involves tradeoffs and constraints that can create disadvantages. Consolidation increases coupling among functional requirements, and processing parameters [8]. It also can reduce access for assembly or maintenance [10, 11]. Moreover, in some cases, it may increase the inputs (e.g., material, labor, or equipment) needed in manufacturing such that costs remain the same or increase compared to a less-consolidated design [12]. These tradeoffs highlight a need to systematically characterize the effects of consolidation on production costs, time, and other manufacturer objectives and determine optimally consolidated designs.

Part consolidation optimization. Prior literature has not developed optimization methods to choose parts for consolidation using AM that considers tradeoffs associated with consolidation. In order to optimize AM consolidation for minimum production costs or time, the following factors must be considered: how to identify candidate components for consolidation, optimize the consolidated parts' build orientation, optimize the layout of consolidated and non-consolidated parts into batches, and estimate and minimize the total production costs or time with respect to the consolidated design. The remaining literature review focuses on related research dealing with these constituent factors, with an emphasis on approaches applied to AM. TABLE 1 summarizes the factors addressed by this body of literature and the unique contributions of our proposed method.

TABLE 1: SUMMARY OF AM CONSOLIDATION RESEARCH.

References	A	B	C	D	E
[12-15]	×				
[13-21]		×			
[38]			×		
Our article	×	×	×	×	×

Annotation:
A: Identify candidates for consolidation
B: Optimize build orientation
C: Determine the effects of consolidation on total production costs and/or time
D: Optimize AM layout to reduce build time and/or costs
E: Optimize the consolidation of parts

Identifying candidates for consolidation. Several design guidelines have been proposed to identify feasible candidates for consolidation [22, 23]. For example, Boothroyd et al. [22] proposed some heuristic rules to find potential candidates for consolidation (e.g., during the operation of the product, does the part move relative to all other parts already assembled?). Yang et al. [23] summarized seven feasibility rules for AM-

enabled consolidation (e.g., assembly access, material availability), and multiple algorithms based on these rules have been developed that seek feasible consolidation candidates. Chadha et al. [24] presented an AM-enabled combination-of-function approach to replace sub-assemblies within a modular product or system with more complex consolidated parts. Yang et al. [25] developed a modularity-based consolidation candidate detection framework based on three principles with regard to the maximum number and the priority of parts to be consolidated. These algorithms generally assess the feasibility of different possible combinations of consolidated parts in an assembly and search for the maximum number of parts that can be consolidated that are feasible.

While the literature discussed above has proposed rules for filtering consolidation candidates for feasibility, prior work has not considered filtering candidates for structural redundancy, meaning that the manufactured part is structurally equivalent (described in detail in section 3.2). Depending on the geometry of parts and their interfaces in an assembly, consolidating certain interfaces while leaving others unconsolidated is nonsensical from a manufacturing standpoint. This is an important consideration for part consolidation optimization because the number of candidates is combinatorial and can explode to large numbers even for assemblies with relatively few parts. Therefore, efficient filtering of the candidates is necessary to reduce the candidates to consider during optimization.

Build orientation optimization. When consolidating parts, the build orientation of the newly consolidated components must be determined. In AM, build orientation is a crucial processing parameter, which affects the surface finish, dimensional accuracy, volumetric error, part strength, production time and cost, and support structures—which are used to uphold internal cavities and overhanging features of a part during build [13, 14]. One key consideration in determining build orientation is to minimize support structures, which directly increase build time, material costs, and the cost and time of post-fabrication steps [15]. The cost effect of support structures is mainly due to the determination of the best build orientation [16]. Support structure minimization by optimizing build orientation has been an extensively researched area in the AM community [17-21].

Layout configuration. Consolidation also affects the layout configuration of parts that are possible during the build. To determine the optimal layout configuration, different types of objective functions have been defined in the literature: (1) fill the build envelope as much as possible [26-32]; (2) minimize build height [29, 30, 32-34]; (3) minimize the volume of support structures [32-34]; (4) minimize surface roughness [32, 34-36]; (5) minimize staircase error [33, 37]; and (6) minimize build time [35-37]. However, optimizing the layout configuration for costs remains an open area of research.

Production cost and time estimation. Many AM cost models have been developed to estimate part cost [15, 38-45]. For example, Rickenbacher et al. [40] developed an integrated cost model, including all pre- and post-processing steps linked to selective laser melting (SLM), to optimize build jobs and to manufacture SLM parts more economically by pooling parts from different projects. Ulu et al. [41] proposed a production cost minimization approach for metal AM (MAM) that concurrently optimizes the part structure and process variables, including beam power and velocity. Johnson and Kirchain [39] determined the production costs of part consolidation in an automotive instrument panel using die-cast magnesium. However, existing research has not examined the influence of part consolidation using AM on production costs or time.

3. METHODOLOGY

The goal of this work is identifying the optimal candidate of part consolidation using MAM that minimizes production cost or time (as specified by the user):

$$\overrightarrow{\mathrm{PC}^{Cost}}^{*} = \min_{\overrightarrow{\mathrm{PC}}} \mathrm{Cost}(\overrightarrow{\mathrm{PC}}, \overrightarrow{\mathbf{Y}}^{*}(\overrightarrow{\mathrm{PC}}), \vec{w}) \qquad (1)$$

$$\overrightarrow{\mathrm{PC}^{Time}}^{*} = \min_{\overrightarrow{\mathrm{PC}}} \mathrm{Time}(\overrightarrow{\mathrm{PC}}, \overrightarrow{\mathbf{Y}}^{*}(\overrightarrow{\mathrm{PC}}), \vec{w}) \qquad (2)$$

where $\overrightarrow{\mathrm{PC}}$ denotes a vector indicating which interfaces are consolidated in a possible candidate design, $\overrightarrow{\mathrm{PC}^{Cost}}$ is the optimal candidate for minimum production cost, $\overrightarrow{\mathrm{PC}^{Time}}$ is the optimal candidate for minimum production time, $\overrightarrow{\mathbf{Y}}^{*}$ is a matrix denoting the optimal build orientation of each part that minimizes their support structures, and $\vec{w}$ denotes a vector including parameters associated with a specific AM process.

As shown in Figure 1, the consolidation optimization method consists of six stages: generation of consolidation candidates, selection of consolidation candidates by filters, the configuration of optimal build orientation and layout, calculation of build time given the MAM processing parameters, evaluation of total production time and costs, and optimization by genetic algorithm.

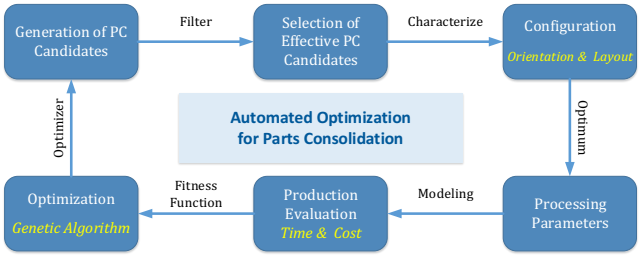

Figure 1: SCHEMATIC DIAGRAM OF THE PRODUCTION EVALUATION METHOD.

3.1 Generation of consolidation candidates

The generation of consolidation candidates for a redesign of a given subsystem begins with identifying the components in the original design and the interfaces between them. For the purposes of this paper, we define the *components* as the original discrete parts in the subsystem design, and the *consolidated parts* as the redesigned parts that are made up of one or more components and each produced as a monolithic part. A *consolidation candidate* is the set of consolidated parts that makeup the subsystem. There are four criteria used to generate consolidation candidates: (1) each component in a consolidated part shares a physical connection (interface) with

at least one other component in the consolidated part unless the part consists of only one component, (2) there is no material variance among components in each consolidated part, (3) there is no relative motion among components in each consolidated part, and (4) any consolidated part does not exceed the size limitation for build. Figure 2 illustrates an example representation of components and interfaces in a network structure of a subsystem consisting of 10 components and 17 interfaces. In this particular example, the subsystem has no material variance or relative motion joints, and its size does not exceed the maximum build envelope, so the only "active" criterion in considering components for consolidation is the first one. Figure 3 shows an example redesign of the subsystem with consolidation reducing the part count to 4.

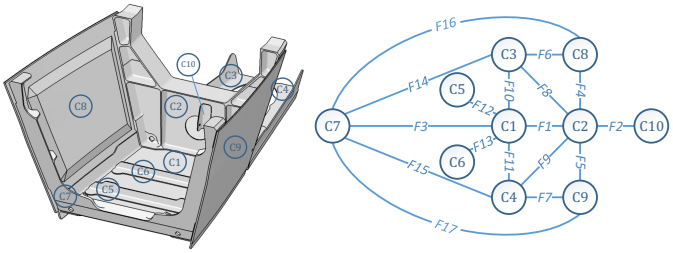

Figure 2: A NETWORK STRUCTURE IDENTIFYING DISCRETE COMPONENTS AND THEIR INTERFACES IN AN EXAMPLE SUBSYSTEM DESIGN (1,043×736×692 MM).

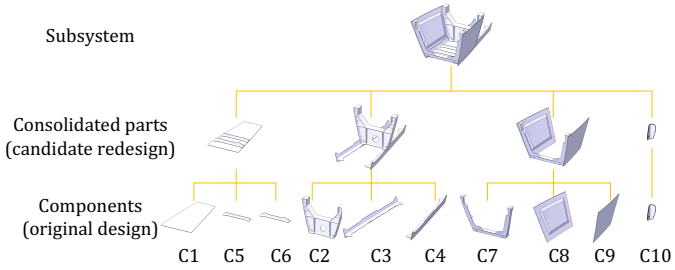

Figure 3: TREE STRUCTURE OF PART CONSOLIDATION. TEN ORIGINAL COMPONENTS ARE CONSOLIDATED INTO FOUR PARTS THAT ARE ASSEMBLED INTO A SUBSYSTEM.

To depict the topological relationship among all components, the connectivity matrix (symmetric adjacency matrix) of the subsystem is shown in Figure 4. The matrix is C x C where C is the number of components in the original design. Each cell represents a physical connection (interface) between two components. Component pairs that share an interface are highlighted in green; and white otherwise. The diagonal cells are in gray and have no meaning (there are no interfaces between a component and itself).

Each consolidation candidate has a one-to-one relationship to an F-digit binary number where F is the total number of interfaces in the original part. Each digit represents the state of the corresponding interface: separation (0) or consolidation (1). The number of all possible consolidation candidates is 2^F in total. If the interface has relative motion or material variance, the digit is set to a fixed state: separation, and the number of candidates is reduced. According to different topological structures (described in Supplemental Material Section A), we can relate the number of interfaces to the number of components with the following bounds:

$$C - 1 \leq F \leq \frac{C(C-1)}{2} \qquad (3)$$

where the lower bound is for a topology in which the fewest possible interfaces are present where each component is still connected to at least one other component, and the upper bound is for a fully connected topology in which all pairs of components have an interface. Here the multiple interfaces between any two components are just considered to be one.

	C1	C2	C3	C4	C5	C6	C7	C8	C9	C10
C1		F1	F10	F11	F12	F13	F3			
C2	F1		F8	F9				F4	F5	F2
C3	F10	F8					F14	F6		
C4	F11	F9					F15		F7	
C5	F12									
C6	F13									
C7	F3		F14	F15				F16	F17	
C8		F4	F6				F16			
C9		F5		F7			F17			
C10		F2								

Figure 4: CONNECTIVITY MATRIX. GREEN CELLS REPRESENT INTERFACES THAT COULD BE CONSOLIDATED. WHITE CELLS REPRESENT UNCONNECTED COMPONENTS.

3.2 Structural redundancy and closed-loop filter

The methodology includes a newly developed filter, which we call a closed-loop filter, to eliminate consolidation candidates that are redundant in terms of generating the same set of parts that are produced as monolithic, rigid structures. As seen in Figure 2, the topological network of the example subsystem includes several strings of three or more components that are all connected together. We call these *ring structures*. For instance, C3-C7-C8 and C1-C4-C7 are two examples of ring structures with three components each, and C1-C3-C8-C2-C0-C4 is a complex ring structure of six components. These ring structures complicate the selection of candidates for consolidation because they can lead to redesigns that do not make sense in practice. To illustrate, consider a subsystem shown in Figure 5 where three components are connected end-to-end across three interfaces that are rigidly joined. This part has $2^3 = 8$ consolidation candidates, which are shown in TABLE 2. However, candidates #4, #6 and #7, each have strictly one "0" in their descriptors, meaning that all components would be produced as a single part but with one of the interfaces left for assembly. If the interfaces are rigidly assembled, and there are no performance criteria (e.g., compliance of the interface) requiring an open interface during assembly into the subsystem or during use, a fully consolidated ring structure will yield strictly better performance than one consolidated with a single separated interface. We define such a consolidated ring-structure, which has one and only separated interface, as *structural redundancy*.

To reduce the convergence time of the consolidation optimization, we develop a *closed-loop filter* that removes all structurally redundant candidates from the selection. If structural redundancy occurs in a complex ring structure (with more than one ring), the one separated interface that causes redundancy must belong to at least one single ring structure. This means that filtering based on single ring structures alone will simultaneously filter for structural redundancy in complex ring structures. Therefore, an inspection of all single rings is sufficient to confirm whether a candidate is structurally redundant.

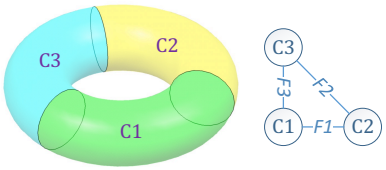

Figure 5: SCHEMATIC DIAGRAM OF A RING STRUCTURE

TABLE 2: CONSOLIDATION CANDIDATES OF A RING STRUCTURE SHOWING STRUCTURAL REDUNDANCY

No.	F1	F2	F3	Redundancy?
1	0	0	0	No
2	0	0	1	No
3	0	1	0	No
4	0	1	1	Yes
5	1	0	0	No
6	1	0	1	Yes
7	1	1	0	Yes
8	1	1	1	No

We find that the closed-loop filter dramatically reduces the number of consolidation candidates that need to be considered. Using the example subsystem shown in Fig 2, after the closed-loop filter is applied, the number of candidates decreases significantly from 2^{17} =131,072 to 4,920. This means nearly 96.5% of candidates are structurally redundant, which greatly reduces the computational burden imposed by the original search space.

3.3 Optimal orientation to minimize support structure

Build orientation influences the volume of the support structures required during the build, which accounts for a large proportion of the production cost and time. The build orientation of the part in our model is optimized to minimize the support structure volume based on the part geometry.

Figure 6 illustrates the volume below a part that requires support structures (represented by green arrows) and how this volume changes with the orientation of the part. The optimal build orientation is defined as the orientation in which the support structure is minimized:

$$\overrightarrow{v^{opt}} = \min_{\vec{v}} V^{sup}(\vec{v}) \tag{4}$$

where $\overrightarrow{v^{opt}}$ is the optimal build orientation, V^{sup}, is the volume of the space taken up by support structures, and $\vec{v}$ is an arbitrary space vector.

Here we propose a simple voxelization-based method to compute the volume of the support structure, V^{sup}, and obtain the optimal build orientation $\overrightarrow{v^{opt}}$ for each part. The voxelization-based method includes four steps: rotation, voxelization, summation, and optimization. The empty domain beneath the geometry is termed as the shadow volume (V^{shadow}). Here we define the support compactness, λ, which is the volume fraction between the support structure volume to the shadow volume, as presented in Equation (5). The support compactness is generally determined by experienced design engineers depending on the material, geometry, and print modality.

$$V^{sup} = \lambda V^{shadow} \tag{5}$$

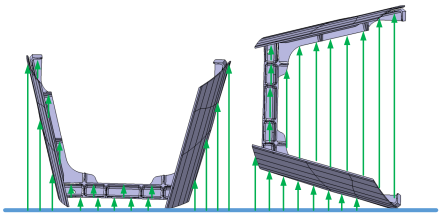

Figure 6: BUILD ORIENTATION INFLUENCES THE SUPPORT STRUCTURE (SHOWN WITH GREEN ARROWS).

(a) Rotation

To minimize support structures, the 3D rotation of a part is parameterized using the three Euler angles as described in [46]. A basic rotation is around one of the axes in a Cartesian coordinate system. The following three basic rotation matrices rotate vectors (point coordinates) by an angle θ around x-, y-, or z-axis, in three dimensions, using the right-hand rules.

$$R_x(\theta) = \begin{bmatrix} 1 & 0 & 0 \\ 0 & \cos(\theta) & -\sin(\theta) \\ 0 & \sin(\theta) & \cos(\theta) \end{bmatrix} \tag{6}$$

$$R_y(\theta) = \begin{bmatrix} \cos(\theta) & 0 & \sin(\theta) \\ 0 & 1 & 0 \\ -\sin(\theta) & 0 & \cos(\theta) \end{bmatrix} \tag{7}$$

$$R_z(\theta) = \begin{bmatrix} \cos(\theta) & -\sin(\theta) & 0 \\ \sin(\theta) & \cos(\theta) & 0 \\ 0 & 0 & 1 \end{bmatrix} \tag{8}$$

In this research, all the geometric models are written in STL files. In a standard STL file, the geometry is represented by three parts: vertex, facet, and facet normal. For a certain rotation from an arbitrary direction (θ_z, θ_y) to the build orientation, any one of the vertex coordinates and facet normal vector in the STL file are transformed by Equation (9).

$$\begin{bmatrix} x \\ y \\ z \end{bmatrix} = R_y(-\theta_y) R_z(-\theta_z) \begin{bmatrix} x_0 \\ y_0 \\ z_0 \end{bmatrix} \tag{9}$$

(b) Voxelization

The rotated part is placed into a minimum bounding cuboid, and then voxelized with a unit length of a. Suppose the cuboid is voxelized into $N_x \times N_y \times N_z$ voxels, so each voxel can be represented by a unique array (i, j, k), where $i = 1,2,\cdots,N_x$, $j = 1,2,\cdots,N_y$, and $k = 1,2,\cdots,N_z$. As shown in Figure 7,

each voxel is colored in one of three colors: green (shadow volume), blue (part material), and yellow (empty space). The positive direction of the Z-axis is defined as up. For a voxel pillar $(i, j, :)$ there are four coloring rules:

(1) If (i, j, k) is in the part or on the surface, then (i, j, k) is part material (blue).

(2) If (i, j, k) is outside the part, and the last one (i, j, N_z) is part material (blue), then (i, j, k) is shadow volume (green).

(3) If (i, j, k) is outside the part, and the last one (i, j, N_z) is not part material (blue), and if the pillar$(i, j, :)$ has at least one voxel that is part material (blue), then the top blue voxel in this pillar is defined as (i, j, K_b), and if $k > K_b$, then (i, j, k) is empty space above the part (yellow), else if $k < K_b$, (i, j, k) is shadow volume (green).

(4) If the whole pillar $(i, j, :)$ has no voxel in the part, then all voxels $(i, j, :)$ are empty space (yellow).

From the figure, it is easy to observe that the part voxels (blue) define the shadow volume (green) by the space beneath or between part material.

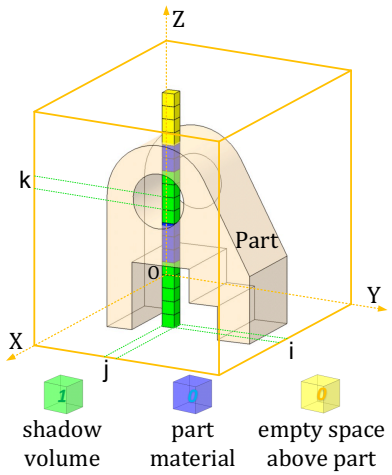

Figure 7: SCHEMATIC DIAGRAM OF VOXELIZATION AND STATE FUNCTION DEFINITION. $\Gamma_{ijk} = 1$ FOR GREEN VOXELS, AND $\Gamma_{ijk} = 0$ FOR BLUE AND YELLOW VOXELS.

(c) Summation

We define a state function to identify the shadow volume by:

$$\Gamma_{ijk} = \begin{cases} 0, & \text{part material or empty space} \\ 1, & \text{shadow volume} \end{cases} \quad (10)$$

The total quantity of voxels in the shadow volume can be written as the summation of Γ_{ijk}, following the expressed in Equation (11). The shadow volume can then be calculated by Equation (12). Figure 8 shows the histogram map of the shadow volume for a rotated part. The height at any point (i, j) is $\sum_{k=1}^{N_z} \Gamma_{ijk}$.

$$M = \sum_{i=1}^{N_x} \sum_{j=1}^{N_y} \sum_{k=1}^{N_z} \Gamma_{ijk} \quad (11)$$

$$V^{shadow} = Ma^3 \quad (12)$$

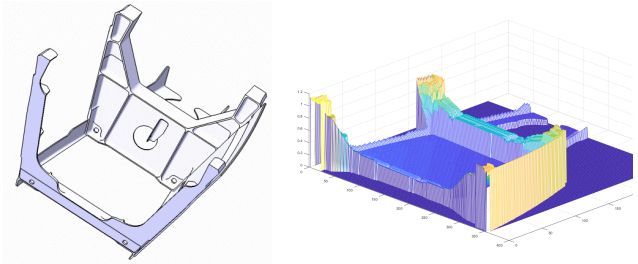

Figure 8: A ROTATED PART $(\theta_z = \pi/4, \theta_y = \pi/4)$ AND HISTOGRAM OF ITS SHADOW VOLUME WITH (θ_z, θ_y).

(d) Orientation optimization

For each part, we compute the shadow volume along the spatial direction (θ_z, θ_y), where $\theta_z \in [0, 2\pi)$ and $\theta_y \in [0, \pi)$ with a step size of $\pi/12$, for a total of 288 directions. The optimal build orientation of the part is the direction with a minimum volume of the support structure. Note that, rotation around the x-axis does not change the shadow volume and so only rotation about the z- and the y-axis is needed to estimate the support structures required for a given part design. (Rotation about the x-axis is considered during the layout of parts into an enclosed volume as discussed in the next section.)

Subsystems with different geometries will vary in the minimum volume of support structures that can be achieved with the optimal orientation. We define a metric that can be used to describe the geometric complexity of a subsystem that contributes to the production costs and time associated with support structures. We call this measure the Shadow Volume Ratio (SVR), which is defined as the ratio between the minimum shadow volume in the optimal build orientation to the total volume of the subsystem.

$$\text{SVR} = \frac{\min(V^{shadow})}{V^{subsystem}} \quad (13)$$

where $V^{subsystem}$ is the net volume of all of the parts in the subsystem, and $\min(V^{shadow})$ is the summation of the minimum shadow volume of all parts in their optimal build orientations.

3.4 Layout configuration by the bottom-left placement approach

Layout optimization of AM parts in batch production is critical for minimizing production cost and time [29, 32, 34]. In this work, we employ a coarse voxelization method to represent parts for layout configuration. In voxelization methods, the unit size of voxels influences the computation time of part generation. The coarse voxelization method is more computationally efficient than other methods using fine voxels, and it can guarantee better packing results than using bounding boxes.

We use the bottom-left (BL) placement approach to optimize the packing of parts into the enclosed build envelope. The target of the layout is to pack all the pieces into the bounding box without overlapping to minimize the length required. The advantages of BL are its speed and simplicity when compared with more sophisticated methods that yield better solutions. As the optimal build orientation of each part

is determined in Section 3.3, the variables in layout configuration are z-rotation degree and (x, y)-position of each part.

For the purposes of this paper, we use 2-D packing into the material build envelope where all parts are placed on the build plate (no stacking of parts). Extension of the methods into 3-D is straight-forward and was considered; however, because the extra support structures that are required for stacking parts contribute significantly to production time and costs, all 3-D packing solutions were dominated by 2-D packing solutions. This is discussed in Supplemental Material Section B.

3.5 Processing parameters of MAM

In this research, we consider two different MAM modalities: open platform systems and enclosed volume systems (Figure 9). Powder-bed fusion (PBF) using EBM is a classic enclosed volume system, using an electron beam to melt metal powder [47]. Directed energy deposition (DED) using EBM is a classic open platform system [48, 49].

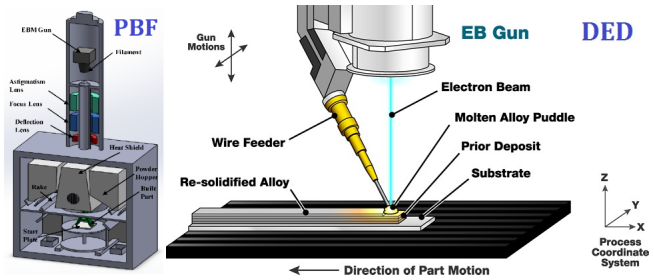

Figure 9: ENCLOSED VOLUME SYSTEM WITH PBF EBM (LEFT; REPRINTED WITH PERMISSION FROM ARCAM [50]) AND OPEN PLATFORM SYSTEM WITH DED EBM (RIGHT; REPRINTED WITH PERMISSION FROM SCIAKY [51]).

The process variables of MAM machines affect production time and cost. Two key parameters that influence our production time and cost models are the depth and width of the melt pool. Assuming the molten pool is semi-circular [52], the depth (d) and width (w) of the molten pool can be computed following [41] as:

$$d = \frac{w}{2} = \sqrt{\frac{2(a_1 \alpha P + a_2)}{\pi v}} \tag{14}$$

where a_1 and a_2 are constants that relate to the material, α is the absorption ratio, P is the heat source (i.e., laser or electron beam) power, and v is the travel speed of the heat source.

3.6 Production evaluation

In this section, we describe our model of the production process from two perspectives: time-based evaluation and cost-based evaluation. The model builds on Ulu et al. [41] as described in Supplemental Material Section C, and all input parameters used in this research are detailed in Supplemental Material Section D.

3.6.1 Time-based evaluation model

The production time model is based on Ulu et al. [41] with additions of support-removal and assembly time models that are newly presented in this paper. The subsystem production time thus includes four elements: build time on the AM machine, setup time between batches, support removal time and assembly time for joining the parts into the subsystem.

$$T^{subsystem} = \sum_r T_r^{build} + \sum_r T_r^{sup-remove} + T^{setup} + T^{assembly} \tag{15}$$

where $T^{subsystem}$ is the total production time for the subsystem, r indexes each part, T_r^{build} is the MAM build time for each part in the subsystem, $T_r^{sup-remove}$ is the support structure removal time for each part, T^{setup} is the per unit setup time to produce a subsystem, and $T^{assembly}$ is the assembly time for a subsystem.

(a) Build time

Following Ulu et al. [38, 41], given the heat source power and travel speed, we can obtain the size of the melt pool. The layer thickness is slightly less than the melt pool depth and can be presented by:

$$l = \beta d \tag{16}$$

where l is the layer thickness, β is a constant ratio ($\beta = 0.9$ for this study) that is based on the electron beam power. The material deposition rate (MDR) ω can be obtained by:

$$\omega = \frac{\frac{w}{2} l}{1/v} = \frac{2(a_1 \alpha P + a_2)\beta v}{v} \tag{17}$$

The build time for each part is determined by summing the build time required for the parts and the required support structures, and accounting for the minimum layer time between two layers, including the transition time (idle time and cooling time) for DED and the recoating time for PBF. Therefore, the build time of each part is:

$$T_r^{build} = T_r^{build-part} + T_r^{build-sup} + T_r^{layer} \tag{18}$$

$$T_r^{build-part} = \frac{V_r^{part}}{\omega} \tag{19}$$

$$T_r^{build-sup} = \frac{V_r^{sup}}{\omega}$$

$$T_r^{layer} = \frac{h_r \, (t^{transition} + t^{recoat})}{l} \tag{20}$$

where V_r^{part} is the volume of the part, V_r^{sup} is the minimum support volume of the part, h_r is the part height, $t^{transition}$ is the transition time between layers for DED, and t^{recoat} is the recoating time between layers for PBF.

(b) Setup time

As each MAM machine has different requirements for build setup, the time associated with the setup is specified for the particular machine. Total setup time is given by:

$$T^{setup} = t^{setup} N^{batch} \tag{21}$$

where t^{setup} is the batch setup time, and N^{batch} is the average number of batches per subsystem, which is determined by the layout configuration.

(c) Support removal time

MAM support structures are usually removed by CNC milling, followed by grinding or polishing the surface of the part formerly attached to the supports, which depends on the product's surface finish requirement [53, 54]. Therefore, the support removal time for each part is:

$$T_r^{sup-remove} = \frac{V_r^{sup}}{MRR} + \frac{A_r^{sup}}{a^{surface}} \tag{22}$$

where V_r^{sup} is the support volume of the part, MRR is the estimated material removal rate (mm^3/s) of CNC milling, A_r^{sup} is the area of surface finishing, and $a^{surface}$ is the surface finishing efficiency (mm^2/s).

(d) Assembly time

Assembly includes machining the interfaces, and joining. Equation (23) below specifies the assembly time for a subsystem that is assembled through riveting. The first term represents machining time of assembly surfaces; and the second, riveting time:

$$T^{assembly} = T^{machining} + T^{riveting} \tag{23}$$

$$T^{machining} = \frac{2}{a^{machining}} \sum_{i=1}^{\mathcal{F}} S_i \tag{24}$$

$$N^{rivet} = \delta^{rivet} \sum_{i=1}^{F} S_i \tag{25}$$

$$T^{riveting} = N^{rivet} t^{riveting} \tag{26}$$

where $\mathcal{F}$ is the number of interface pairs after consolidation, S_i is the area of the i^{th} interfaces between parts, $a^{machining}$ is the machining efficiency (mm^2/s) on machining the interfaces, δ^{rivet} is the surface distribution density of rivets, N^{rivet} is the total quantity of rivets, and $t^{riveting}$ is the time to complete a single riveting.

3.6.2 Cost-based evaluation model

The per unit production costs include the input costs (e.g., material, labor, and equipment) associated with MAM setup (C^{setup}), build and post-processing for parts (C^{part}), and assembly ($C^{assembly}$). The part cost consists of part material cost ($C_r^{part-mat}$), support material cost (C_r^{sup}), machine and maintenance cost ($C^{machine}$), scrap material cost - e.g., powder lost during recovery and recycling (C^{scrap}), and energy consumption cost (C^{energy}).

$$C^{subsystem} = C^{part} + C^{setup} + C^{assembly} \tag{27}$$

$$C^{part} = \sum_r C_r^{part-mat} + \sum_r C_r^{sup} + C^{machine} + C^{scrap} + C^{energy} \tag{28}$$

For the production cost model, we follow Ulu et al. [38, 41] in accounting for the cost of the build, setup, material for the part, energy use, scrap, and machine costs. Details are described in Supplemental Material Section C. We add to this model the cost of building and removing support structures as well as the cost of assembly steps as described below.

(a) Support structure cost

The support structure cost contains material cost ($C^{sup-mat}$) and support removal cost ($C^{sup-remove}$). The material used for the support structure is usually the same as the part material. Support removal cost ($C^{sup-remove}$) is given as the product of labor price and the support removal time.

$$C_r^{sup} = C_r^{sup-mat} + C_r^{sup-remove} \tag{29}$$

$$C_r^{sup-mat} = p^{sup-mat} \rho^{sup-mat} V_r^{sup} \tag{30}$$

$$C_r^{sup-remove} = p^{labor} T_r^{sup-remove} \tag{31}$$

where $p^{sup-mat}$ is the support material price ($/kg), $\rho^{sup-mat}$ is the support material density (kg/m^3), p^{labor} is labor price ($/h).

(b) Assembly cost

Assembly cost includes machining cost and riveting cost. The riveting cost contains material (rivet) cost and labor cost. All items are given by:

$$C^{assembly} = C^{machining} + C^{riveting} \tag{32}$$

$$C^{machining} = p^{machining} T^{machining} \tag{33}$$

$$C^{riveting} = p^{rivet} N^{rivet} + p^{labor} T^{riveting} \tag{34}$$

where $p^{machining}$ is the user cost of capital of the CNC machine ($/h), p^{rivet} is the riveting material price ($/rivet), and the remaining parameters are defined in section 3.6.1.

3.7 Optimization by Genetic Algorithm

For those subsystems with relatively few interfaces, the optimal consolidation candidate can be obtained by complete enumeration over all possible candidates. However, as the number of interfaces increases, the candidates increase exponentially. For example, a subsystem with 94 interfaces has $2^{94} \approx 1.98\times10^{28}$ candidates. To solve the problem for those subsystems with a large number of interfaces, we develop a genetic algorithm (GA) that determines which components to consolidate to reduce production time or costs.

Figure 10 displays the flow-chart of the algorithm. The input is the connectivity matrix of a subsystem with initial components and interfaces and its STL file. In the GA, we encode each consolidation candidate with a chromosome of length equal to the number of interfaces, *F,* specified in the

connectivity matrix, as shown in Figure 11. An initial population of consolidation candidates is generated by randomly generating chromosomes. The closed-loop filter is employed to remove the redundant candidates for each iteration. Production time or cost is used as the fitness function (as specified by the user), which depends on an inner loop that determines the optimal orientation to minimize support structures and layout of the parts into batches during the build.

Each iteration of the GA consists of five phases. (1) *Initialization:* The process begins with a set of the population that includes 100 candidates that have passed through the closed-loop filter. (2) *Fitness Function:* The production cost or time is employed as the fitness function (as specified by the user) to evaluate each candidate. (3) *Evaluation and Selection:* Based on the ranking of cost or time, we use the Roulette Wheel Selection method to select candidates and allow them to pass their genes to the next generation [55]. (4) *Crossover:* Single-point crossover is used to combine the genetic information of two parents to generate new children. (5) *Mutation:* Thirty percent of children are selected and subjected to a mutation with a low probability of 2%. Iterations are terminated when a specified maximum number of generations is reached. The specified maximum number of generations was verified to converge to the optimum within a small percentage tolerance as described in section 4.2 and in Supplemental Material Section E.

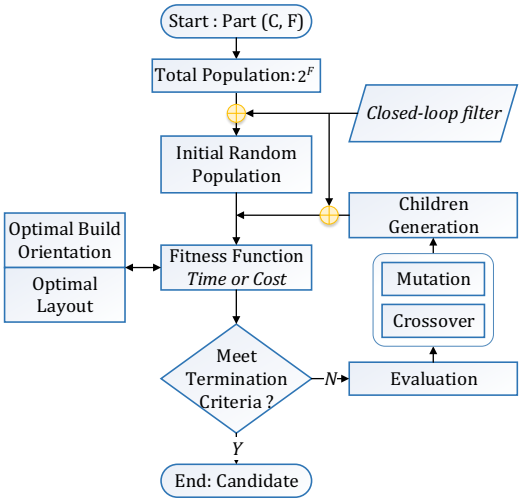

Figure 10: FLOWCHART OF GA.

Figure 11: A BINARY ENCODED CHROMOSOME HOLDING INFORMATION ON INTERFACE CONSOLIDATION.

4. OPTIMIZATION RESULTS

We demonstrate the developed method on a test-bed subsystem selected in collaboration with a company in the aircraft industry. The subsystem is an aft fairing, which is composed of 48 parts and 94 interfaces assembled by rivet joints. We simulate the fairing as being produced from Ti-6-Al-4V through both PBF EBM and DED EBM processes, respectively. The input parameters for these simulations are expressed in detail in Supplemental Material Section D. The parameters are derived from literature detailing operating conditions and cost estimates from industrial MAM production facilities [56], as well as equipment suppliers [51]. It is important to note that the cost estimates do not include costs associated with overhead, management, production plant construction, transportation, or inventory.

Using a subset of the fairing that has a smaller number of components, we first test the GA by comparing results to the global optimum determined by complete enumeration. We then use the GA on the full fairing to find optimal components to consolidate for minimum production costs and time.

4.1 Global optima

The small-scale part (a subsystem of the fairing) has 2^{17} consolidation candidates in total. Using the closed-loop filter, these candidates are reduced to only 4,920. In the case of minimizing production time, the optimum for both PBF and DED is the same. The solution is to consolidate nine of the original 10 components (shown in Figure 12): C1-C8 and C10 are consolidated into one part, and C9 is produced discretely. The unit production time for PBF is reduced from 77 hours for the original unconsolidated design to 58 hours. For DED, the unit production time is reduced from 54 hours to 43 hours because of the larger input power and travel speed available in this case. For both cases, MAM build accounts for more than 90% of the production time, with assembly accounting for 5% or less.

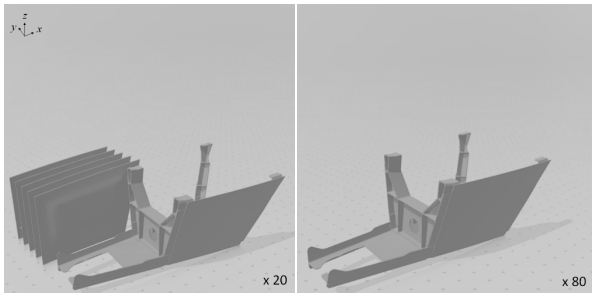

Figure 12: TIME-BASED AND COST-BASED OPTIMALLY CONSOLIDATED PARTS FOR PBF (PRODUCTION VOLUME: 100).

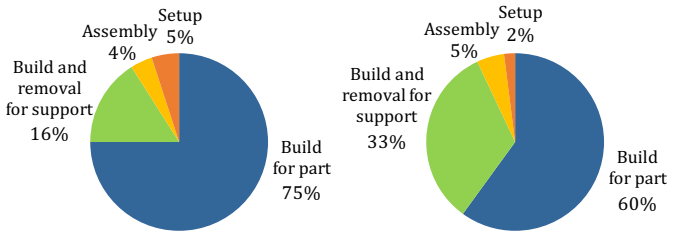

Figure 13: PRODUCTION TIME CONTRIBUTORS OF THE OPTIMALLY CONSOLIDATED FAIRING FOR PBF (LEFT) AND DED (RIGHT)

The optimal consolidation candidates for minimum production cost are shown in Figure 14 for PBF and Figure 15 for DED. The solution for DED has three parts: (C2-C10, C1-C3-C4-C5-C6, and C7-C8-C9) with the unit production costs

of $9,486. The PBF solution reduces costs from $20K to $16K per unit. In both cases, over 80% of costs are from part material, MAM build (machine costs, maintenance, and labor), and support structure material build and removal (Figure 16). For PBF, the optimally consolidated design has four parts: (C2-C10, C1-C4-C5-C6, C7-C8-C9, and C3). This is because titanium powder, which is used in the PBF case, is significantly more expensive than titanium wire used in the DED case. The increased material price moves the optimum to consolidate fewer parts so that less support structure material is needed to uphold these smaller discrete parts during the build.

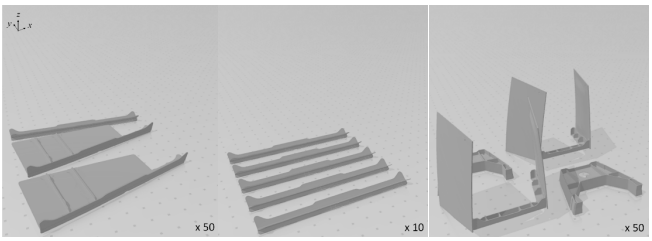

Figure 14: COST-BASED OPTIMAL CONSOLIDATION CANDIDATE WITH FOUR PARTS FOR PBF (ANNUAL PRODUCTION VOLUME: 100).

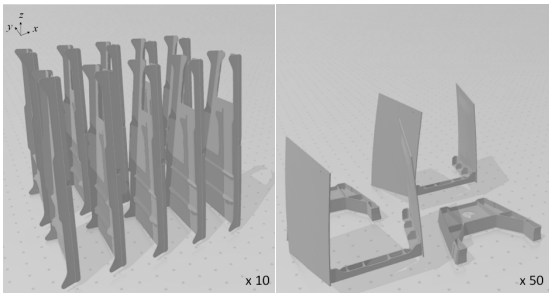

Figure 15: COST-BASED OPTIMAL CONSOLIDATION CANDIDATE WITH THREE PARTS FOR DED (ANNUAL PRODUCTION VOLUME: 100).

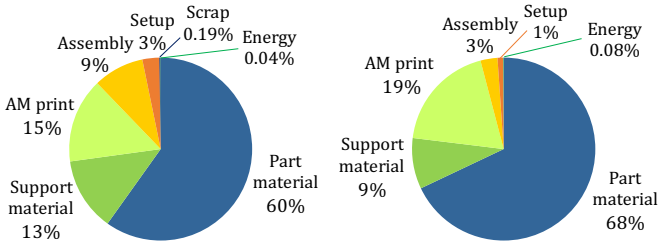

Figure 16: PRODUCTION COST CONTRIBUTORS OF THE OPTIMALLY CONSOLIDATED FAIRING FOR PBF (LEFT) AND DED (RIGHT)

4.2 Consolidation optimization of small-scale part

Here we test the performance of the developed GA on optimizing the small-scale part (as shown in Figure 2) for optimal consolidation. Figure 17 displays the estimated PBF unit production cost of each feasible consolidation candidate after filtering, which is computed through complete enumeration. The GA solution is determined with the crossover percentage set to 80%, the mutation percentage set to 30%, and the mutation rate set to 2%. Ten candidates are randomly selected for the initial population, and the algorithm is run until the fifth generation. Five tests repeating this process are conducted to compare solutions to the global optimum. As shown in Table 3, the GA results converge to within 3% of the global optimum in all of these tests.

We also use the algorithm to optimize the consolidation of the full fairing system that consists of 48 components and 94 interfaces, yielding a total of 2^{94} ($\approx 1.98\times10^{28}$) total consolidation candidates. Convergence results show that both the time and cost curves flatten at about the 80th generation. Results are described in detail in Supplemental Material Section E.

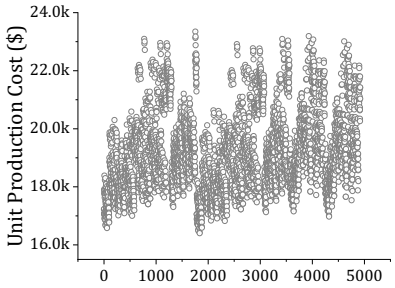

Figure 17: COST VALUES OF ALL FILTERED CANDIDATES OF THE SUBSYSTEM BY PBF EBM.

TABLE 3: GROUND TRUTH GLOBAL OPTIMUM AND GA RESULTS.

Items	Target	Test 1	Test 2	Test 3	Test 4	Test 5
Sequence	1838	1808	1783	80	1838	45
Number of parts	4	7	8	6	4	7
Cost ($1,000)	16.22	16.38	16.56	16.73	16.22	16.68

5. Key tradeoff within the test-bed problems

An important tradeoff was observed in the test-bed problems between the number of parts consolidated, and production costs and time. In this section, we characterize these tradeoffs to understand the main determinants of the optimally consolidated design.

We create a metric to characterize the extent of consolidation in a subsystem and relate the metric to production time and costs. The degree of consolidation (DOC) is defined as the ratio of the number of consolidated interfaces, F^{con}, in a redesigned system to the number of original interfaces, F:

$$\text{DOC} = \frac{F^{con}}{F} \tag{35}$$

The DOC is in the interval [0,1]. F^{con} ranges from zero to F, where a value of zero represents the original (unconsolidated) subsystem design and $F^{con} = F$ represents a fully consolidated subsystem that is produced as one monolithic part.

The quantitative tradeoff between the DOC and production cost and time in the fairing subsystem are shown in

Figure 18. The figure shows each consolidation candidate (in white) as well as the Pareto frontier that minimizes time and cost, respectively, for a particular value of the DOC (in red). As the DOC increases, both time and cost decrease at first and then increase. This illustrates that the optimal DOC is an interior solution.

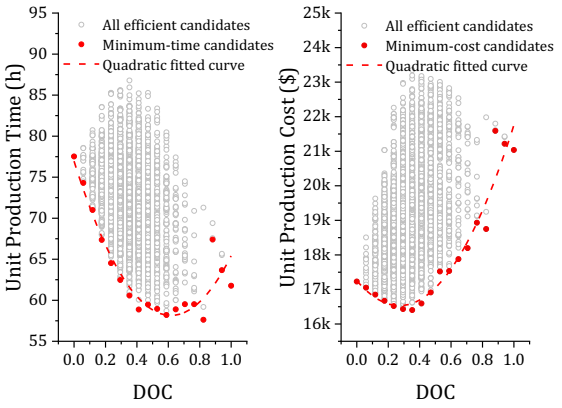

Figure 18: UNIT PRODUCTION TIME AND COST VARIATIONS WITH DOC (SUPPORT COMPACTNESS = 0.1, PBF EBM).

In Figure 19, we plot the constituent factors influencing the tradeoff between the DOC and unit production time and costs. As seen in the figure, the fundamental tradeoff is between reducing assembly (and to a lesser extent setup) steps and increasing support structures. As the fraction of consolidated interfaces increases, the number of assembly and setup steps decreases, reducing the associated production time and costs. However, more support structures are needed to uphold the larger consolidated parts, increasing the build time to construct the support structures and the costs associated with support material and build time. This creates an interior solution of the DOC between 0% and 100%.

We also find that the optimal DOC decreases with increasing support compactness. A detailed characterization of these results is available in the Supplemental Material Section F.

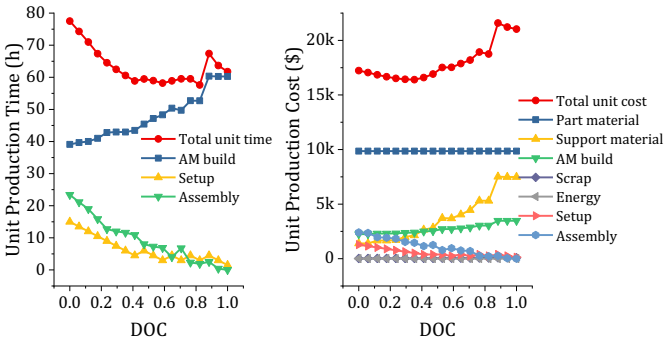

Figure 19: MINIMUM TIME AND COST VARIATIONS WITH DOC (SUPPORT COMPACTNESS = 0.1, PBF EBM).

Note that, in Figure 19 (b), the part material is constant with DOC. This is because the presented methodology does not consider the topological redesign of parts after consolidation so that the material contained in the parts (not including support structure material or scrap) remains approximately the same. The mass of rivets or welding seams that are eliminated with consolidation is negligible with respect to the whole subsystem.

6. Generalization of the identified tradeoffs

In this section, we provide a logical rationale and supporting evidence justifying that the tradeoffs we observe between the optimal degree of consolidation, support structures, and assembly steps are generalizable to many different types of subsystems. We discuss how the magnitude of the tradeoffs depends on the shadow volume ratio of the subsystem, material price and print modality, and the type of joining process used in the assembly, and how these factors affect the optimal degree of consolidation. We then find the optimal DOC in a variety of different subsystems to verify that the presented rationale can explain differences in the optima for different geometries, material, print modalities, and assembly requirements.

As we found in the test-bed subsystem (summarized in Figure 18 and Figure 19), the optimal DOC depends on the tradeoffs between the support structures that are needed to uphold the consolidated parts and the time or cost to assemble the parts. These tradeoffs appear to be inherent to the consolidation of many different types of subsystems using MAM. Part consolidation decreases the number of discrete parts in the subsystem, reducing the time and costs of assembly and build setup. However, as more components are consolidated, they can no longer be individually oriented to minimize support structures; their orientations are now constrained together. As a result, the optimal build orientation for the consolidated part often requires more support structures than the optimum for the unconsolidated components. Therefore, with an increase in the degree of consolidation, the cost (or time) associated with building and removing the support structures generally increases. The one exception is if the optimal orientation of the consolidated part requires the same amount of support structures as the sum of the support structures needed for the unconsolidated components. For example, this would be the case if the consolidated subsystem could be oriented to have zero support structures, or if the optimal orientation of the consolidated subsystem was the same as the optimal orientation of the discrete components.

Figure 20 illustrates a conceptual schematic of how the optimal degree of consolidation is influenced by different subsystems with different shadow volume ratios, material prices and deposition rates, and assembly requirements. As the figure shows, the optimal DOC for minimizing production cost (or time) moves toward no consolidation if the optimal orientation of the subsystem has a larger shadow volume, and toward full consolidation as the shadow volume decreases. The optimum also depends on material cost and deposition rates as well as the cost (or time) of the required assembly operations. If the material cost is relatively low (e.g., using Aluminum or Stainless Steel instead of Titanium, or wire instead of powder), or deposition rates are faster, the optimum

will move toward more consolidation. If the cost (or time) of the assembly operations is relatively lower (e.g., welding instead of riveting), the optimum will move toward less consolidation.

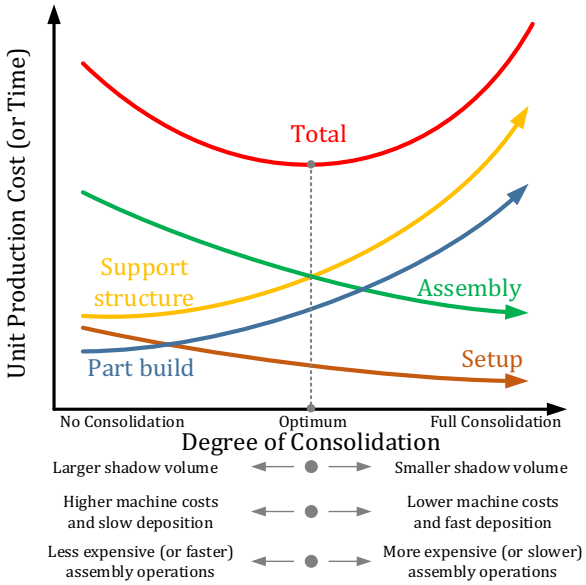

Figure 20: KEY TRADEOFFS AFFECTING THE OPTIMAL DEGREE OF CONSOLIDATION

To verify the application of this generalized framework of the key tradeoffs influencing the optimal degree of consolidation, we apply our optimization approach to three very different products in addition to the test-bed subsystem. Specifically, we optimize a puzzle plane, a toy chair, and a heart valve in addition to the aircraft fairing. These products were selected because of their variation in structural complexity in terms of the shadow volume ratio. The size and SVR of each product are shown just below their CAD diagrams in

TABLE **4**. The plane, toy chair, and heart valve are all assembled with welding whereas the puzzle plane, toy chair, and heart valve are assumed to be assembled with welding whereas the aircraft fairing is riveted together. We examine four different scenarios for each of these products: producing them with Ti6Al4V or Al-6061, and using PBF or DED.

In the following sections, we describe how the shadow volume ratio, material and print modality, and product size influence the optimal DOC results.

(a) Shadow volume effect

As is shown in

TABLE **4** the products with a higher SVR, such as the fairing subsystem and the puzzle plane, have an interior optimal DOC. By contrast, the toy chair—which has a smaller SVR—has a local interior minimum but its global minimum is full consolidation. Products with a very small shadow volume, such as the heart valve, have monotonically decreased production time and costs with respect to DOC. The optimal candidate, in this case, is full consolidation. In general, products with a higher SVR *ceterus paribus* will have smaller optimal DOCs for minimum production cost and time.

(b) Material and print modality effects

The aluminum and titanium alloys have different thermophysical properties and material prices. According to Equations (17)-(18) the build time ratio of the two materials can be given by Equation (36). It can be seen that the build time of the aluminum alloy is nearly equal to that of the titanium alloy. However, aluminum has a cheaper material price and is faster to rivet or weld than titanium, so unit production cost and time using the aluminum alloy is less than the titanium alloy.

$$\frac{(T^{build})_{Al}}{(T^{build})_{Ti}} = \frac{(a_1 \alpha P + a_2)_{Ti}}{(a_1 \alpha P + a_2)_{Al}} \approx 1.006 \qquad (36)$$

As expected,

TABLE **4** shows that when using the titanium alloy, the slope of the production cost and time curves with respect to the DOC decrease. As a result, the optimal DOC for the aircraft fairing and puzzle plane are larger when using aluminum than using titanium. In the toy chair and heart valve cases, the optima remain at 100%.

(c) Model size effect

As mentioned in Section 6.1, the enlargement of the shadow volume shifts the optimal DOC toward less consolidation while the enlargement of assembly costs (or time) shifts the optimum point toward more consolidation. These tradeoffs have interesting implications for the relationship between the size of the product and the optimal DOC. The support structure cost (and time) is proportional to the cube of the size, while the assembly cost (and time) is roughly proportional to the square of the size. When the subsystem is scaled up, the support structure cost (and time) increases faster than the assembly cost (and time), and the optimal DOC shifts toward less consolidation.

As shown in TABLE 5, the fairing subsystem model is scaled up and down, respectively, in order to study the tradeoffs between variations of size and optimal DOC. The comparison of the three sizes reveals that scaling up the fairing size to 5 times its original size shifts the DOC to 0%, while scaling down the fairing size by one-fifth shifts it to 100%.

7. Conclusions

In this paper, we present the first AM part consolidation optimization method that considers the tradeoff between consolidation and manufacturer objectives. Using an objective function of minimizing production costs or time, the method generates and filters consolidation candidates through a connectivity matrix, determines optimal build orientation, layout, and finds the optimally consolidated design using a GA we develop that encodes each candidate by the interfaces that are consolidated.

Using an aircraft fairing as a test-bed, we compare results for minimum production time and costs, respectively, for two scenarios: PBF EBM and wire-fed DED EBM. The fundamental tradeoff in both these cases is between reducing assembly (and to a lesser extent setup) steps and increasing

support structures. As the fraction of consolidated interfaces increases, the number of assembly and setup steps decreases, reducing the associated production time and costs. However, more support structures are needed to uphold the larger consolidated parts, increasing the build time to construct the support structures and the costs associated with support material and build time, and support removal. The cost-optimal design for DED has fewer parts than PBF because the metal wire is less expensive than powder, and therefore the additional costs of building support structures are smaller.

We present a rationale and evidence that supports that the identified tradeoffs generalize to many different types of products. As more interfaces are consolidated, additional support structures are often required for the larger parts, which are more difficult to orient to reduce support structures compared to smaller parts. This increase in support structures drives up production time (due to longer build times) and costs (due to support material and removal costs) which rival reductions in assembly time and costs. We find that products that are smaller, have relatively smaller shadow volume ratios, lower material costs, or more expensive or time-consuming assembly operations will have an optimum closer to 100% consolidation.

The model and testbed results presented in this article are based on MAM, especially PBF EBM and DED EBM. Applications to polymer AM are outside the scope of the paper. Additionally, the presented methodology and results do not consider the topological redesign of parts after consolidation, which is left to future work. Topological redesign of parts would be expected to reduce material use and build time of consolidated parts, leading to optimal levels of consolidation that are higher to some extent than the presented results.

Acknowledgment

This research was supported in part by Carnegie Mellon University's Manufacturing Futures Institute and by an aircraft manufacturing company. The authors gratefully thank the company representatives who collaborated on the project.

TABLE 4: INFLUENCE OF TOPOLOGY, MATERIAL, AND MAM MODALITY ON OPTIMAL DEGREE OF CONSOLIDATION.

Model	Topology	Ti6Al4V	Al-6061
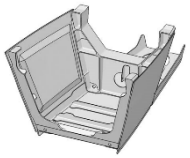 1,043×736×692 mm SVR = 7.59	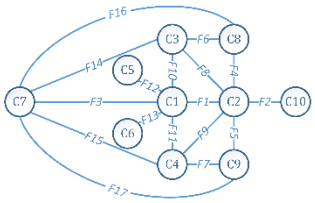	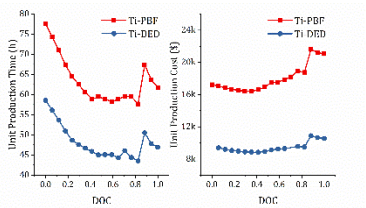	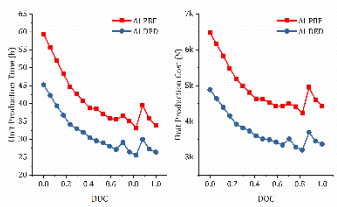
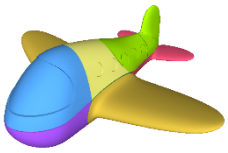 1,058×1,246×415 mm SVR = 0.477	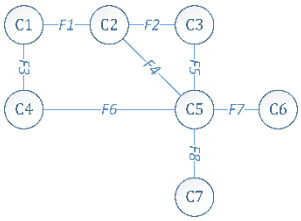	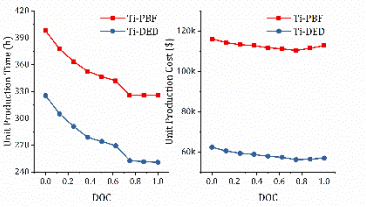	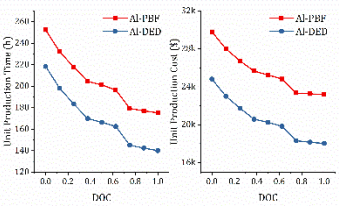
 173×61×47 mm SVR = 0.2272	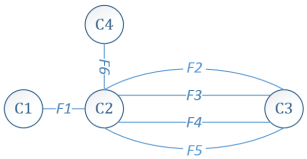	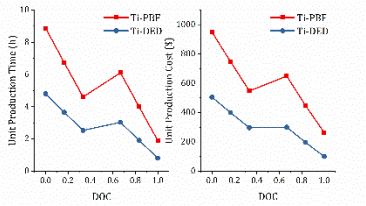	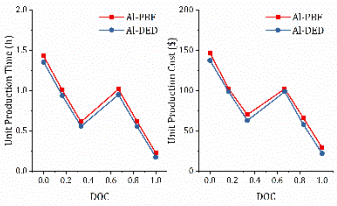
 20×8×8 mm SVR = 0	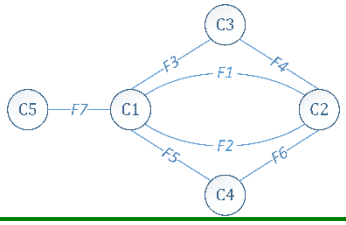	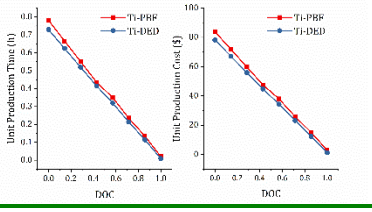	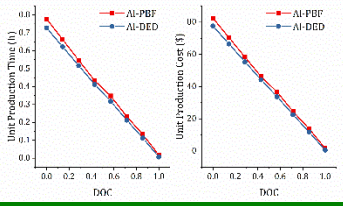

TABLE 5: SUBSYSTEM SIZE EFFECT ON OPTIMAL DEGREE OF CONSOLIDATION.

Model	Ti6Al4V	Al-6061
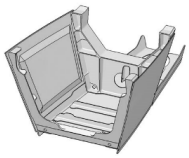 Original Size	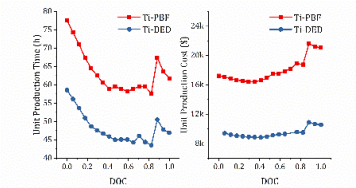	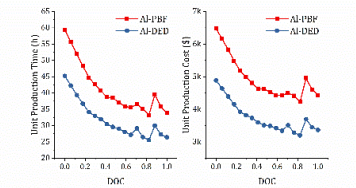
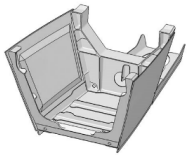 5X Size	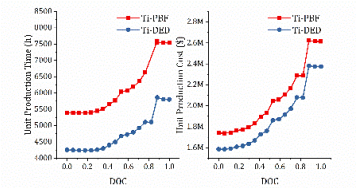	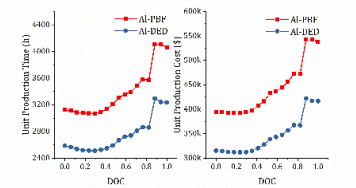
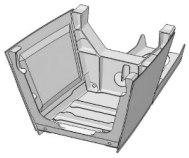 0.2X Size	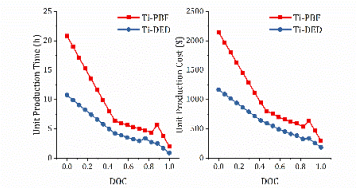	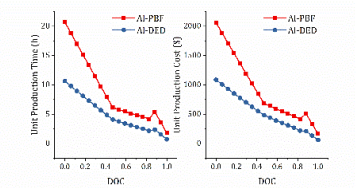

References

[1] Yang, S., Talekar, T., Sulthan, M. A., and Zhao, Y. F., 2017, "A Generic Sustainability Assessment Model towards Consolidated Parts Fabricated by Additive Manufacturing Process," Procedia manufacturing, 10, pp. 831-844.

[2] Yang, S., Tang, Y., and Zhao, Y. F., 2015, "A new part consolidation method to embrace the design freedom of additive manufacturing," Journal of Manufacturing Processes, 20, pp. 444-449.

[3] Yang, S., and Zhao, Y. F., 2015, "Additive manufacturing-enabled design theory and methodology: a critical review," The International Journal of Advanced Manufacturing Technology, 80(1), pp. 327-342.

[4] Hague, R., 2006, "Unlocking the design potential of rapid manufacturing," Rapid manufacturing: an industrial revolution for the digital age.

[5] Uriondo, A., Esperon-Miguez, M., and Perinpanayagam, S., 2015, "The present and future of additive manufacturing in the aerospace sector: A review of important aspects," Proceedings of the Institution of Mechanical Engineers, Part G: Journal of Aerospace Engineering, 229(11), pp. 2132-2147.

[6] Wong, K. V., and Hernandez, A. J. I. M. E., 2012, "A review of additive manufacturing," ISRN Mechanical Engineering, 2012.

[7] Schmelzle, J., Kline, E. V., Dickman, C. J., Reutzel, E. W., Jones, G., and Simpson, T. W., 2015, "(Re) Designing for part consolidation: understanding the challenges of metal additive manufacturing," Journal of Mechanical Design, 137(11), p. 111404.

[8] Frey, D., Palladino, J., Sullivan, J., and Atherton, M., 2007, "Part count and design of robust systems," Systems engineering, 10(3), pp. 203-221.

[9] Türk, D.-A., Kussmaul, R., Zogg, M., Klahn, C., Leutenecker-Twelsiek, B., and Meboldt, M., 2017, "Composites part production with additive manufacturing technologies," Procedia CIRP, 66, pp. 306-311.

[10] Booker, J., Swift, K., and Brown, N., 2005, "Designing for assembly quality: strategies, guidelines and techniques," Journal of Engineering design, 16(3), pp. 279-295.

[11] Boothroyd, G., Dewhurst, P., and Knight, W. A., 2001, Product Design for Manufacture and Assembly, revised and expanded, CRC press.

[12] Combemale, C., Whitefoot, K. S., Ales, L., and Fuchs, E. R., 2018, "Not All Technological Change is Equal: Disentangling Labor Demand Effects of Automation and Parts Consolidation," Available at SSRN 3291686.

[13] Taufik, M., and Jain, P. K., 2013, "Role of build orientation in layered manufacturing: a review," International Journal of Manufacturing Technology and Management, 27(1-3), pp. 47-73.

[14] Jibin, Z., "Determination of optimal build orientation based on satisfactory degree theory for RPT," Proc. Computer Aided Design and Computer Graphics, 2005. Ninth International Conference on, IEEE, p. 6 pp.

[15] Thomas, D. S., and Gilbert, S. W., 2014, "Costs and cost effectiveness of additive manufacturing," Special Publication, NIST.

[16] Alexander, P., Allen, S., and Dutta, D., 1998, "Part orientation and build cost determination in layered manufacturing," Computer-Aided Design, 30(5), pp. 343-356.

[17] Langelaar, M., 2016, "Topology optimization of 3D self-supporting structures for additive manufacturing," Additive Manufacturing, 12, pp. 60-70.

[18] Leary, M., Merli, L., Torti, F., Mazur, M., and Brandt, M., 2014, "Optimal topology for additive manufacture: a method for enabling additive manufacture of support-free optimal structures," Materials & Design, 63, pp. 678-690.

[19] Mirzendehdel, A. M., and Suresh, K., 2016, "Support structure constrained topology optimization for additive manufacturing," Computer-Aided Design, 81, pp. 1-13.
[20] Paul, R., and Anand, S., 2015, "Optimization of layered manufacturing process for reducing form errors with minimal support structures," Journal of Manufacturing Systems, 36, pp. 231-243.
[21] Vanek, J., Galicia, J. A. G., and Benes, B., "Clever support: Efficient support structure generation for digital fabrication," Proc. Computer graphics forum, Wiley Online Library, pp. 117-125.
[22] Boothroyd, G., Dewhurst, P., and Knight, W. A., 2001, Product Design for Manufacture and Assembly, CRC press.
[23] Yang, S., Santoro, F., and Zhao, Y. F., 2018, "Towards a numerical approach of finding candidates for additive manufacturing-enabled part consolidation," Journal of mechanical design, 140(4), p. 041701.
[24] Chadha, C., Crowe, K., Carmen, C., and Patterson, A., 2018, "Exploring an AM-enabled combination-of-functions approach for modular product design," Designs, 2(4), p. 37.
[25] Yang, S., Santoro, F., Sulthan, M. A., and Zhao, Y. F., 2019, "A numerical-based part consolidation candidate detection approach with modularization considerations," Research in Engineering Design, 30(1), pp. 63-83.
[26] Nyaluke, A., Nasser, B., Leep, H. R., and Parsaei, H. R., 1996, "Rapid prototyping work space optimization," Computers and industrial engineering, 31(1-2), pp. 103-106.
[27] Canellidis, V., Dedoussis, V., Mantzouratos, N., and Sofianopoulou, S., 2006, "Pre-processing methodology for optimizing stereolithography apparatus build performance," Computers in industry, 57(5), pp. 424-436.
[28] Wodziak, J. R., Fadel, G. M., and Kirschman, C., "A genetic algorithm for optimizing multiple part placement to reduce build time," Proc. Proceedings of the Fifth International Conference on Rapid Prototyping, University of Dayton Dayton, OH, pp. 201-210.
[29] Zhang, X., Zhou, B., Zeng, Y., and Gu, P., 2002, "Model layout optimization for solid ground curing rapid prototyping processes," Robotics and Computer-Integrated Manufacturing, 18(1), pp. 41-51.
[30] Hur, S.-M., Choi, K.-H., Lee, S.-H., and Chang, P.-K., 2001, "Determination of fabricating orientation and packing in SLS process," Journal of Materials Processing Technology, 112(2-3), pp. 236-243.
[31] Canellidis, V., Giannatsis, J., and Dedoussis, V., 2013, "Efficient parts nesting schemes for improving stereolithography utilization," Computer-Aided Design, 45(5), pp. 875-886.
[32] Zhang, Y., Gupta, R. K., and Bernard, A., 2016, "Two-dimensional placement optimization for multi-parts production in additive manufacturing," Robotics and Computer-Integrated Manufacturing, 38, pp. 102-117.
[33] Gogate, A., and Pande, S., 2008, "Intelligent layout planning for rapid prototyping," International Journal of Production Research, 46(20), pp. 5607-5631.
[34] Wu, S., Kay, M., King, R., Vila-Parrish, A., and Warsing, D., "Multi-objective optimization of 3D packing problem in additive manufacturing," Proc. IIE Annual Conference. Proceedings, Institute of Industrial and Systems Engineers (IISE), p. 1485.
[35] Pandey, P. M., Thrimurthulu, K., and Reddy, N. V., 2004, "Optimal part deposition orientation in FDM by using a multicriteria genetic algorithm," International Journal of Production Research, 42(19), pp. 4069-4089.
[36] Thrimurthulu, K., Pandey, P. M., and Reddy, N. V., 2004, "Optimum part deposition orientation in fused deposition modeling," International Journal of Machine Tools and Manufacture, 44(6), pp. 585-594.
[37] Phatak, A. M., and Pande, S. S., 2012, "Optimum part orientation in rapid prototyping using genetic algorithm," Journal of manufacturing systems, 31(4), pp. 395-402.
[38] Huang, R., Ulu, E., Kara, L. B., and Whitefoot, K. S., "Cost Minimization in Metal Additive Manufacturing Using Concurrent Structure and Process Optimization," Proc. ASME 2017 International Design Engineering Technical Conferences and Computers and Information in Engineering Conference, American Society of Mechanical Engineers, pp. V02AT03A030-V002AT003A030.
[39] Johnson, M., and Kirchain, R., 2009, "Quantifying the effects of parts consolidation and development costs on material selection decisions: A process-based costing approach," International Journal of Production Economics, 119(1), pp. 174-186.
[40] Rickenbacher, L., Spierings, A., and Wegener, K., 2013, "An integrated cost-model for selective laser melting (SLM)," Rapid Prototyping Journal, 19(3), pp. 208-214.
[41] Ulu, E., Huang, R., Kara, L. B., and Whitefoot, K. S., 2018, "Concurrent Structure and Process Optimization for Minimum Cost Metal Additive Manufacturing," Journal of Mechanical Design.
[42] Baumers, M., Dickens, P., Tuck, C., and Hague, R., 2016, "The cost of additive manufacturing: machine productivity, economies of scale and technology-push," Technological forecasting social change, 102, pp. 193-201.
[43] Dinda, S., Modi, D., Simpson, T. W., Tedia, S., and Williams, C. B., "Expediting Build Time, Material, and Cost Estimation for Material Extrusion Processes to Enable Mobile Applications," Proc. ASME 2017 International Design Engineering Technical Conferences and Computers and Information in Engineering Conference, American Society of Mechanical Engineers, pp. V02AT03A034-V002AT003A034.
[44] Ruffo, M., Tuck, C., and Hague, R., 2006, "Cost estimation for rapid manufacturing-laser sintering production for low to medium volumes," Proceedings of the Institution of Mechanical Engineers, Part B: Journal of Engineering Manufacture, 220(9), pp. 1417-1427.
[45] Yim, S., and Rosen, D., "Build time and cost models for additive manufacturing process selection," Proc. ASME 2012 international design engineering technical conferences and computers and information in engineering conference, American Society of Mechanical Engineers, pp. 375-382.
[46] Ulu, E., Korkmaz, E., Yay, K., Ozdoganlar, O. B., and Kara, L. B., 2015, "Enhancing the structural performance of additively manufactured objects through build orientation optimization," Journal of Mechanical Design, 137(11), p. 111410.

[47] Gong, H., Rafi, K., Gu, H., Starr, T., and Stucker, B., 2014, "Analysis of defect generation in Ti–6Al–4V parts made using powder bed fusion additive manufacturing processes," Additive Manufacturing, 1, pp. 87-98.
[48] Murr, L. E., Gaytan, S. M., Ramirez, D. A., Martinez, E., Hernandez, J., Amato, K. N., Shindo, P. W., Medina, F. R., and Wicker, R. B., 2012, "Metal fabrication by additive manufacturing using laser and electron beam melting technologies," Journal of Materials Science and Technology, 28(1), pp. 1-14.
[49] Nie, Z., Wang, G., McGuffin-Cawley, J. D., Narayanan, B., Zhang, S., Schwam, D., Kottman, M., and Rong, Y. K., 2016, "Experimental Study and Modeling of H13 Steel Deposition Using Laser Hot-Wire Additive Manufacturing," Journal of Materials Processing Technology, 235, pp. 171-186.
[50] Toh, W. Q., Wang, P., Tan, X., Nai, M. L. S., Liu, E., and Tor, S. B., 2016, "Microstructure and wear properties of electron beam melted Ti-6Al-4V parts: A comparison study against as-cast form," Metals, 6(11), p. 284.
[51] Inc., S., 2015, "Advantages of Wire AM vs. Powder AM," http://www.sciaky.com/additive-manufacturing/wire-am-vs-powder-am.
[52] Gockel, J., Beuth, J., and Taminger, K., 2014, "Integrated control of solidification microstructure and melt pool dimensions in electron beam wire feed additive manufacturing of Ti-6Al-4V," Additive Manufacturing, 1-4, pp. 119-126.
[53] Chen, N., and Frank, M. C., "A method for metal AM support structure design to facilitate removal," Proc. Solid Freeform Fabrication, pp. 1516-1524.
[54] Vaidya, R., and Anand, S. J. P. M., 2016, "Optimum support structure generation for additive manufacturing using unit cell structures and support removal constraint," 5, pp. 1043-1059.
[55] Jebari, K., and Madiafi, M., 2013, "Selection methods for genetic algorithms," International Journal of Emerging Sciences, 3(4), pp. 333-344.
[56] Inc., S., 2016, "EBAM 300 Series," https://www.aniwaa.com/product/3d-printers/sciaky-ebam-300-series/.

Supplemental Material for "Optimization of Part Consolidation for Minimum Production Costs and Time Using Additive Manufacturing"

Zhenguo Nie, Sangjin Jung, Levent Burak Kara, Kate S. Whitefoot

Carnegie Mellon University

A. INTERFACE BOUNDS

A number of components (C) are connected into one single part through a number of interfaces (F). Given a fixed number of components, the structures that have the minimum number of interfaces will have $F = \binom{C}{C-1} = C - 1$ interfaces. An example of this type of structure is the single linked chain shown in FIGURE 1. The structures that have the maximum number of interfaces will have $F = \binom{C}{2} = \frac{C(C-1)}{2}$ interfaces, as shown in FIGURE 2.

Single chain: all in line

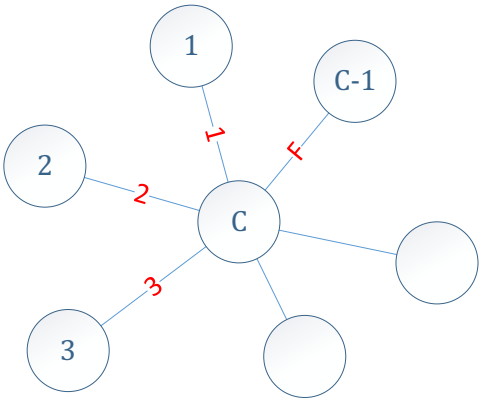

Single chain: radical pattern

FIGURE 1: THE SINGLE LINKED CHAIN WITH MINIMUM INTERFACES

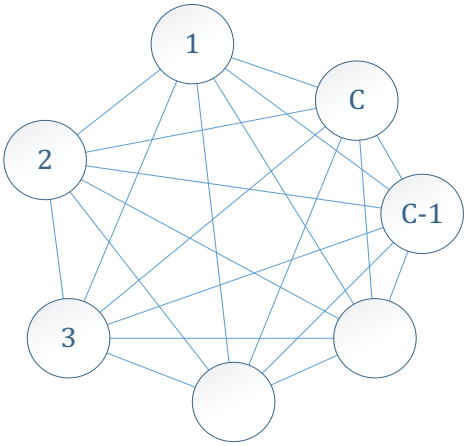

FIGURE 2: FULLY CONNECTED NETWORK WITH MAXIMUM INTERFACES

B: TRADEOFF ON THE LAYOUT CONFIGURATION

For demonstrative purposes, FIGURE 3 shows three cases of comparison between a 2D ground layout and a 3D layout of generic shapes. The thin solid lines represent support structures, and the blue solid blocks represent parts. Based on this simple comparison, we can see that in these cases, the 3D layout needs more support structures than the ground layout. This observation motivates our examination of whether using ground layout, which is more computationally efficient, dominates the 3D layout in terms of finding the lowest production cost (or time) layout solutions.

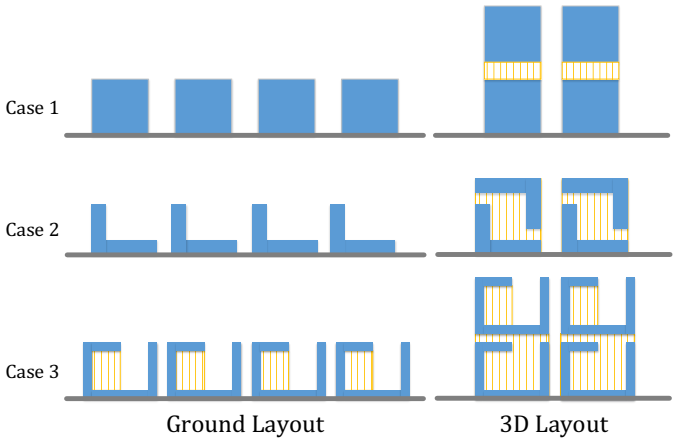

FIGURE 3: COMPARISON OF THE SUPPORT STRUCTURE BETWEEN GROUND LAYOUT AND 3D LAYOUT IN THE FRONT VIEW.

We can conceptualize the cases where ground layout solutions will dominate 3D layout by considering a larger enough build envelop size where we begin placing parts in the envelope (i.e., in a batch) starting from zero. As parts are placed in the envelope, it lowers

production costs (and time) to place them on the build plate (to avoid support structures) until there is no more room to lay them directly on the plate and they must be stacked. Until this threshold, a 2D ground layout could be used to place the parts. If we continue to add parts, the latter parts will be placed over the former parts, and then a 3D layout configuration must be used. As shown in FIGURE 4, if the minimum cost (or time) number of parts in the batch is past the threshold (represented as the vertical dashed line), then a 3D layout is needed. However, if the optimum does not cross the threshold, we can use a ground layout to save computational time. We would expect the optimum to be close to the threshold, because in the ground layout period, increasing the number of parts can bring down production costs (and time), because of reduced batches and setup-time. Once the threshold is crossed and parts are stacked, additional support structures are needed that increase costs (and time).

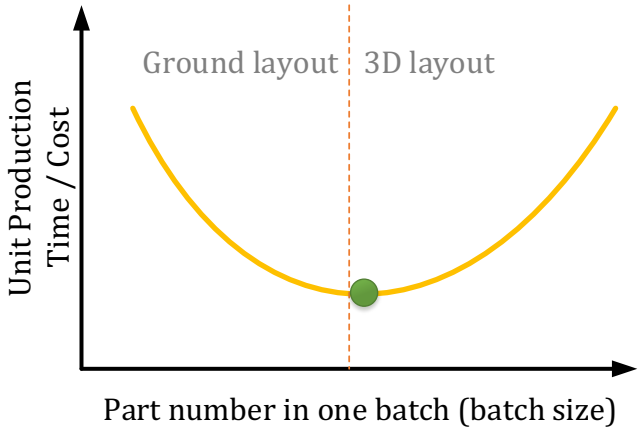

FIGURE 4: SCHEMATIC OF THE LAYOUT CONFIGURATION THRESHOLD.

FIGURE 5 plots the results of production time and costs as a function of the Pareto frontier of the number of parts in a batch for the aircraft fairing subsystem. According to Section 4.2, the optimal candidate for minimum (PBF) production time has two parts: $[C1-C8,\ C10]$, $[C9]$, and the optimal candidate for the minimum (PBF) production cost has four parts: $[C2, C10]$, $[C1, C4-6]$, $[C7-C9]$, $[C3]$. Suppose 10 sets of parts are manufactured by PBF, and the build envelop size of PBF machine is $1.25 \times 1.25 \times 1.25$ (m). The batch size (the number of parts in one batch) starts from one, and can be up to ten, which is the capacity limitation for the build envelop. The optimal per subsystem unit production time (DOC = 0.82) and production cost (DOC=0.36) are shown in the figure. As the figure shows, the optimal points of both the time and cost curves are located on the threshold line between ground layout and 3D layout. We can therefore use a ground layout in this case to reduce computational convergence time.

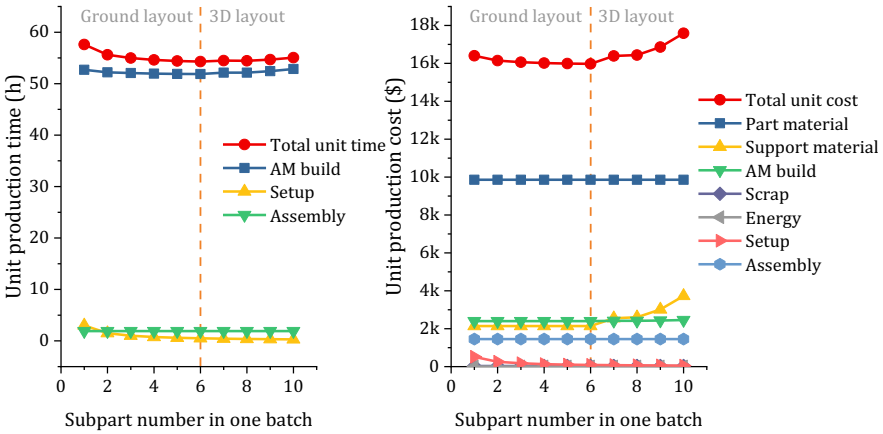

FIGURE 5: TIME AND COST VARIATIONS IN LAYOUT.

C: PRODUCTION COST EVALUATION MODEL

As described in the main body of the paper, the subsystem production costs are determined from the following equations.

$$C^{subsystem} = C^{part} + C^{setup} + C^{assembly} \tag{1}$$

$$C^{part} = \sum_{r} C_r^{part-mat} + \sum_{r} C_r^{sup} + C^{machine} + C^{scrap} + C^{energy} \tag{2}$$

(a) Part material cost

The part material cost contains the cost of the material needed for the final form of the part, but does not include the cost of other material needed to build the part, namely the support structure and scrap material [1].

$$C_r^{part-mat} = p^{material} \rho^{material} V_r^{part} \tag{3}$$

where $p^{material}$ is the material price (\$/kg), $\rho^{material}$ is the material density (kg/m^3).

(b) Support structure cost

The support structure cost contains support material cost ($C^{sup-mat}$) and support removal cost ($C^{sup-remove}$). The material of the support structures is usually identical with the part material in AM. Support removal cost ($C^{sup-remove}$) is given as the product of the price of labor and the support removal time.

$$C_r^{sup} = C_r^{sup-mat} + C_r^{sup-remove} \tag{4}$$

$$C_r^{sup-mat} = p^{sup-mat} \rho^{sup-mat} V_r^{sup} \tag{5}$$

$$C_r^{sup-remove} = p^{labor} T_r^{sup-remove} \tag{6}$$

where $p^{sup-mat}$ is the support material price ($/kg), $\rho^{sup-mat}$ is the support material density (kg/m^3), p^{labor} is labor price ($/h).

(c) Scrap cost

The material lost during manufacturing, for example powder lost during powder recovery and recycling, is referred to as scrap. The scrap cost is given by [1]:

$$C^{scrap} = p^{material}\rho^{material}\eta V^{envelope} \tag{7}$$

where $V^{envelope}$ is the sum of the build envelope volume for all batches required to produce one unit of the subsystem, and η is the scrap rate.

(d) Machine cost

The machine cost includes the amortized equipment cost, machine maintenance cost, and the labor cost required to operate the machinery [1]:

$$C^{machine} = A^{machine}T^{build} \tag{8}$$

$$A^{machine} = \frac{C^{invest} + C^{maintain}L}{LH} + p^{labor} \tag{9}$$

where T^{build} is the build time, C^{invest} is the machine investment cost, $C^{maintain}$ is annual machine maintenance cost, L is the lifetime of the machine, H is the annual operation time.

(e) Energy cost

The energy cost comes from two parts: electricity consumption for the AM machine during production and idle electricity consumption when the AM machine is not printing [1].

$$C^{energy} = p^{elec}\left(\int_0^{T^{build}} Pdt + P_0T^{build}\right) \tag{10}$$

where p^{elec} is the electricity price ($/kW · h), P is the actual power of the AM machine, P_0 is the idle power.

(f) Setup cost

The setup cost contains the labor cost and the machine cost during the setup process, given by:

$$C^{setup} = A^{machine}T^{setup} \tag{11}$$

(g) Assembly cost

Assembly cost includes machining cost and riveting cost. The riveting cost contains material (rivet) cost and labor cost. All items are given by:

$$C^{assembly} = C^{machining} + C^{riveting} \tag{12}$$

$$C^{machining} = p^{machining} T^{machining} \tag{13}$$

$$C^{riveting} = p^{rivet} N^{rivet} + p^{labor} T^{riveting} \tag{14}$$

D: INPUT PARAMETERS

Tables 1-2 list the input parameters for the PBF EBM and DED EBM cases, respectively. Table 3 lists the remaining MAM and assembly input parameters used in both cases.

TABLE 1: INPUT PARAMETERS OF PBF EBM.

Parameter	Magnitude	Unit	Annotation
C^{invest}	1.1E6	$	PBF EBM machine investment [1]
$C^{maintain}$	5.0E4	$	PBF EBM machine maintenance [1]
$p^{material}$	250	$/kg	Ti6Al4V powder [1]
$p^{material}$	58	$/kg	Al alloy 6061 powder [2]
P	2.0	kW	Power [1]
t^{recoat}	6	s	Recoating time [3]
t^{setup}	1.5	h	Unit setup time [1]
v	16.9	mm/s	Travel speed [1]
η	1	%	Scrap rate [1]

TABLE 2: INPUT PARAMETERS OF DED EBM

Parameter	Magnitude	Unit	Annotation
C^{invest}	2.5E5	$	DED EBM machine investment [4]
$C^{maintain}$	1.5E4	$	DED EBM machine maintenance [4]
$p^{material}$	128	$/kg	Ti6Al4V wire G5 [5]
$p^{material}$	30	$/kg	Al 6061 wire-1.75mm [6]
P	2.5	kW	Power [4]
$t^{transition}$	10	s	Transition time
t^{setup}	1	h	Unit setup time [4]
v	25.4	mm/s	Travel speed [4]
η	0	%	Scrap rate [7]

TABLE 3: TEST-BED SYSTEM INPUT PARAMETERS FOR MAM PRODUCTION AND ASSEMBLY

Parameter	Magnitude	Unit	Annotation
a_1	8.25E-11	$m^3/W \cdot s$	P-V coefficient of Ti6Al4V [1]
	1.29E-10		P-V coefficient of Al alloy [8]
a_2	-2.44E-8	m^3/s	P-V coefficient of Ti6Al4V [1]
	-1.46E-9		P-V coefficient of Al alloy [8]
$a^{machining}$	30	mm^2/s	Machining efficiency [9]
$a^{surface}$	0.5	mm^2/s	Surface working efficiency
H	7000	h/year	Annual working time [1]
L	7	year	Lifetime of the machine [1]
p^{elec}	0.03	$/kW · h	Unit electric cost [1]

p^{labor}	28	\$/h	Labor cost per unit time [1]
$p^{machining}$	150	\$/h	Machining cost per unit time [10]
p^{rivet}	1.97	\$	Unit rivet cost (BACB30FN5-4) [11]
$p^{welding}$	200	\$/h	Welding cost per unit time [12]
P_0	2000	W	Initial power [1]
MRR	100	mm^3/s	Removal rate of support [13]
$t^{riveting}$	120	s	Unit riveting time [14]
α	0.90	-	Absorption ratio of Ti6Al4V [15]
	0.50	-	Absorption ratio of Al alloy [15]
β	0.90	-	Layer thickness ratio [1]
δ^{rivet}	2755.56	$1/m^2$	Distribution density of rivets [14]
λ	0.10	-	Support compactness of support [16]
$\rho^{material}$	4.50E3	kg/mm^3	Density of Ti6Al4V [17]
	2.70E3		Density of Al alloy [17]

E: PART CONSOLIDATION OPTIMIZATION OF AN AIRCRAFT FAIRING

The consolidation of the whole aircraft fairing subsystem was optimized for the PBF EBM scenario using the developed GA. As shown in FIGURE 6, the full fairing consists of 48 components and 94 interfaces, yielding a total of 2^{94} ($\approx 1.98 \times 10^{28}$) total consolidation candidates. An initial population of five hundred randomly selected candidates were used to breed the next generation and 100 generations in total were populated. The crossover percentage is set to 80%, the mutation percentage is set to 30%, and the mutation rate is set to 2%. Convergence results for both minimum production costs and minimum production time, respectively, are shown in FIGURE 7. It is observed that both the time and cost curves flatten at about the 80th generation.

The computational time to convergence of the algorithm depends on the subsystem size and topology, the number of components, and the voxel size. In our results, the computional time for the fairing system takes approximately 5 days to converge with a voxel size of 2 mm. The smaller sized product case studies presented in the paper in Table 4 take considerably less time for convergence. The puzzle plane example converges in 6 hours with a voxel size of 10 mm. The chair example takes 1 hour with a voxel of 1 mm, and the heart valve takes 5 minutes with a voxel size of 1 mm. All the computations were conducted with a dual Intel Core i7-9700 CPU.

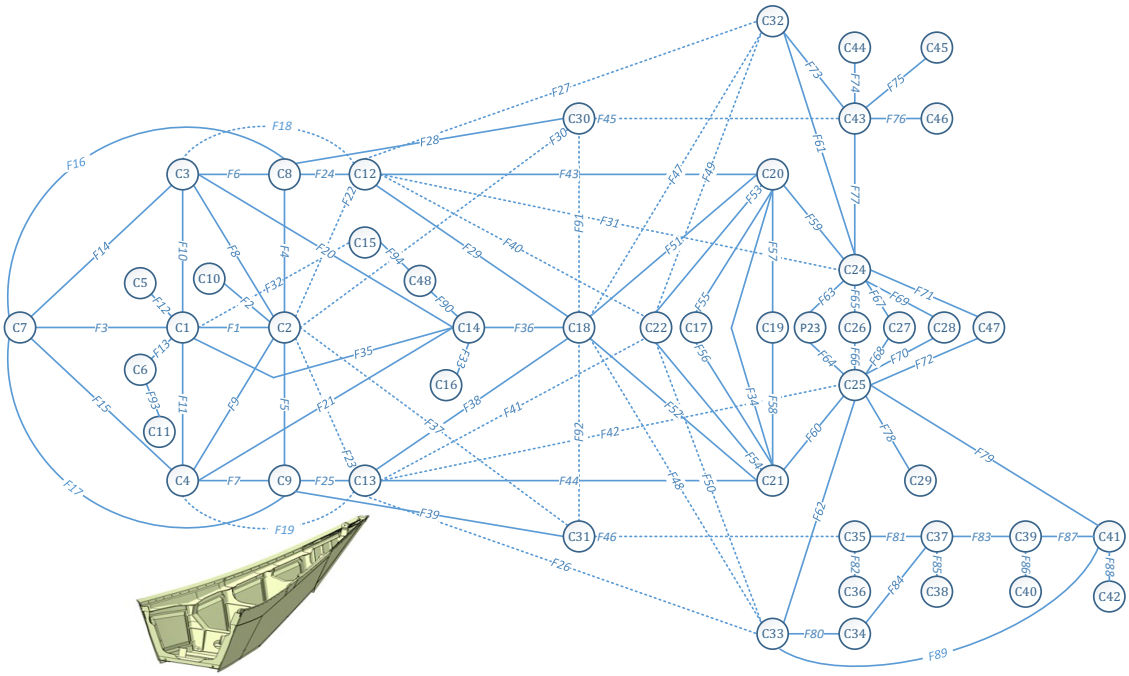

FIGURE 6: THE CONNECTIVITY DIAGRAM OF THE FAIRING WITH 48 COMPONENTS AND 94 INTERFACES. PART SIZE: 3,176 × 736 × 692 MM.

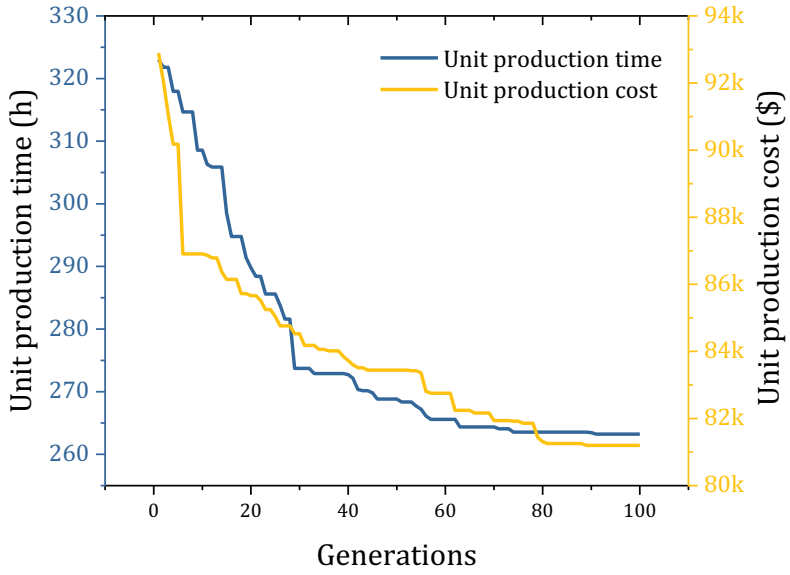

FIGURE 7: GA CONVERGENCE RESULTS OF PRODUCTION TIME AND PRODUCTION COST FOR THE AIRCRAFT FAIRING.

The minimum production time solution, shown in FIGURE 8, consolidates the 48 parts into three. This reduces the per unit production time from 323 hours to 263 hours. The

minimum production time solution is to consolidate the 48 components to three parts: [C1,C2,C4-30,C32-34,C37-39,C41-48], [C3,C7,C14], [C31,C35-37,C39,C40].

The minimum production cost solution, shown in FIGURE 9, has five consolidated parts: [C1-22,C31,C48], [C23,C25,-29,C33,C34,C37-39,C41,C42,C47], [C30,C32,C43-46], [C23,C24,C27,C28,C47], [C35-37,C39,C40]. Similarly to the subsystem fairing solution, the minimum cost solution has more discrete parts because the material required to build support structures for larger consolidated parts is expensive. Therefore, the minimal cost solution has slightly more and smaller parts that require less support structure in total and somewhat longer assembly time than the minimal time solution. The minimum cost consolidation design reduces the unit production costs from $92,900 to approximately $81,200.

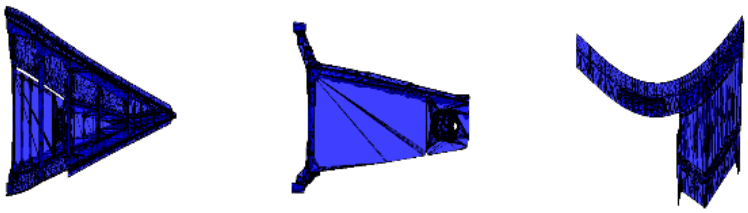

FIGURE 8: THE OPTIMAL CANDIDATE WITH THREE PARTS FOR MINIMUM (PBF) PRODUCTION TIME (THE BUILD ORIENTATION IS PERPENDICULAR AND OUTWARD TO THE PLANE OF THE PAPER).

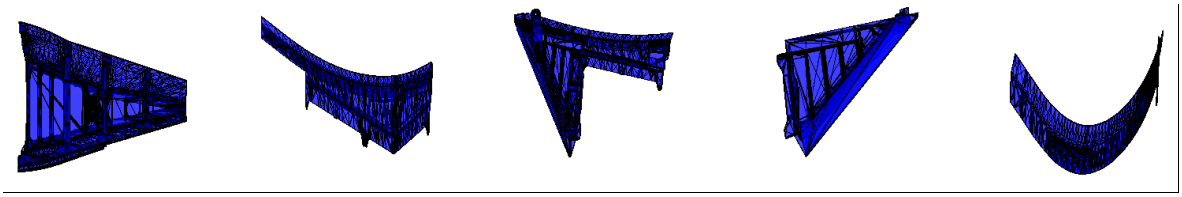

FIGURE 9: THE OPTIMAL CANDIDATE WITH FIVE PARTS FOR MINIMUM (PBF) PRODUCTION COST (THE BUILD ORIENTATION IS PERPENDICULAR AND OUTWARD TO THE PLANE OF THE PAPER).

F. SENSITIVITY ANALYSIS OF THE SUPPORT COMPACTNESS

To understand the relationship between support structures and minimum time and cost consolidation solutions, we conduct a sensitivity analysis of the optimal results on support compactness. FIGURE 10 shows how the minimum production time and cost varies when the support compactness ranges from zero—where no support structures are needed—to 0.5—where 50% of the support volume is taken up by the support material. It can be seen that both time and cost increase substantially with support compactness. This underscores the importance of reducing support compactness (within the limit of ensuring the necessary support structure strength) to bring down production time and costs.

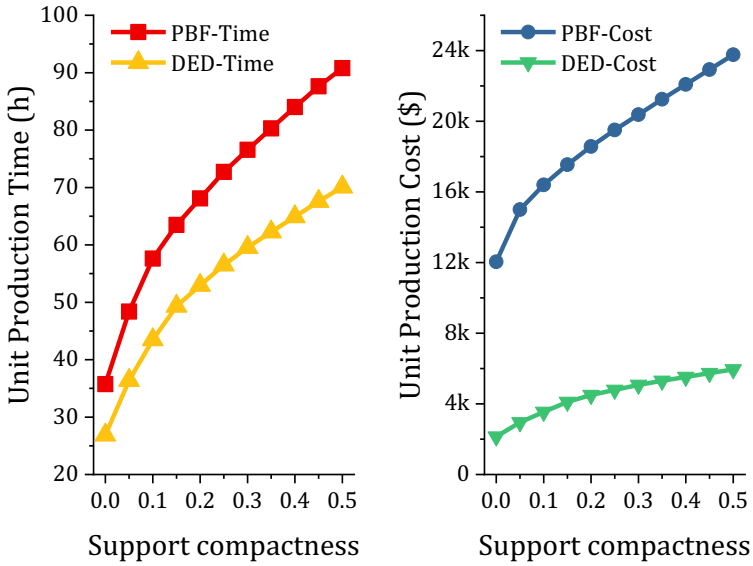

FIGURE 10: TIME AND COST VARIATIONS WITH SUPPORT COMPACTNESS.

For a better understanding of how the optimal degree of consolidation (DOC) varies with the support compactness, the MAM print modality, and manufacturer objective function, we compute optimal DOC variations with support compactness in four different scenarios shown in FIGURE 11. As expected, the optimal DOC has a negative correlation with the support compactness because if more support structure material is needed, the optimum will move to consolidate fewer interfaces. We also find that the time-based optimal DOC is often larger than the cost-based solution in the products we study. This reflects that the cost of building and removing the additional support structures required for more consolidated designs is larger relative to the reduced assembly costs than the additional time is relative to reduced assembly time. In addition, the DED-cost solution has a larger optimal DOC than the PBF-cost solution, while DED-time and PBF-time have almost the same optimal DOC based on our input parameters. The larger optimal DOC for the DED-cost solution is due to the lower material price of titanium wire relative to powder.

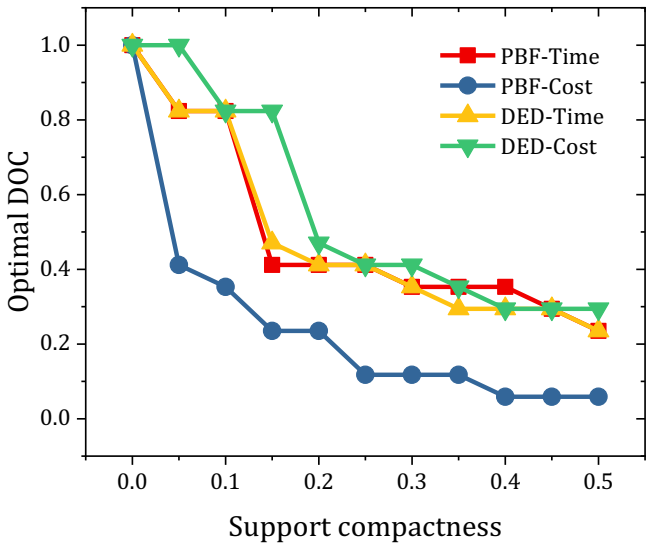

FIGURE 11: OPTIMAL DOC VARIATIONS WITH SUPPORT COMPACTNESS FOR EACH OF THE MINIMUM TIME AND MINIMUM COST SOLUTIONS FOR THE PBF CASE AND THE DED CASE.

REFERENCES

[1] Ulu, E., Huang, R., Kara, L. B., and Whitefoot, K. S., 2019, "Concurrent Structure and Process Optimization for Minimum Cost Metal Additive Manufacturing," Journal of Mechanical Design, 141(6), pp. 061701-061701-061710.

[2] Engineers, A. E., 2018, "ALUMINUM POWDER, ATOMIZED," https://micronmetals.com/products/aluminum-powder-atomized/.

[3] McMillan, M., Leary, M., and Brandt, M., 2017, "Computationally efficient finite difference method for metal additive manufacturing: A reduced-order DFAM tool applied to SLM," Materials and Design, 132, pp. 226-243.

[4] Inc., S., 2016, "EBAM 300 Series," https://www.aniwaa.com/product/3d-printers/sciaky-ebam-300-series/.

[5] Inc., S., 2015, "Advantages of Wire AM vs. Powder AM," http://www.sciaky.com/additive-manufacturing/wire-am-vs-powder-am.

[6] Amazon, 2018, "SainSmart 1.75 Aluminum Metal 1.75 mm Filament for 3D Printing," https://www.amazon.com/SainSmart-Aluminum-Metal-Filament-Printing/dp/B017SGCX2G/ref=sr_1_1?keywords=1.75+Aluminum+Metal+1.75+mm+Filament+for+3D+Printing&qid=1553902481&s=industrial&sr=1-1.

[7] Nie, Z., Wang, G., McGuffin-Cawley, J. D., Narayanan, B., Zhang, S., Schwam, D., Kottman, M., and Rong, Y. K., 2016, "Experimental study and modeling of H13 steel deposition using laser hot-wire additive manufacturing," Journal of Materials Processing Technology, 235, pp. 171-186.

[8] Li, Y., and Gu, D., 2014, "Parametric analysis of thermal behavior during selective laser melting additive manufacturing of aluminum alloy powder," Materials and Design, 63, pp. 856-867.

[9] Chen, X., Öpöz, T. T. J. P., and Research, M., 2016, "Effect of different parameters on grinding efficiency and its monitoring by acoustic emission," 4(1), pp. 190-208.

[10] Kennewell, 2018, "Pricing Guide," http://www.kennewell.com/products/pricing-guide/.

[11] Military-fasteners, 2018, "BACB30FN5-4," https://military-fasteners.com/rivets/pin_rivets/BACB30FN5-4.

[12] Thumbtack, 2018, "Metalworkers on Thumbtack cost," https://www.thumbtack.com/p/welding-cost.

[13] Yazdi, M. R. S., and Chavoshi, S. Z. J. P. E., 2010, "Analysis and estimation of state variables in CNC face milling of AL6061," 4(6), pp. 535-543.

[14] Petrova, A., and Lukina, N. J. P. S. S. D., 2008, "Adhesive technologies in aircraft construction," 1(2), pp. 83-90.
[15] Trapp, J., Rubenchik, A. M., Guss, G., and Matthews, M. J., 2017, "In situ absorptivity measurements of metallic powders during laser powder-bed fusion additive manufacturing," Applied Materials Today, 9, pp. 341-349.
[16] Hao, L., Raymont, D., Yan, C., Hussein, A., and Young, P., 2011, "Design and additive manufacturing of cellular lattice structures," The International Conference on Advanced Research in Virtual and Rapid Prototyping (VRAP). Taylor & Francis Group, Leiria, pp. 249-254.
[17] MatWeb, 2018, "MatWeb, Your Source for Materials Information," http://www.matweb.com/.